

A Unifying Perspective of Common Motifs That Occur across Disparate Classes of Materials Harboring Displacive Phase Transitions

Anna Grünebohm, Andreas Hütten, Anna E. Böhmer, Jan Frenzel, Ilya Eremin, Ralf Drautz, Inga Ennen, Luana Caron, Timo Kuschel, Frank Lechermann, Dario Anselmetti, Thomas Dahm, Frank Weber, Kai Rossnagel, and Gabi Schierning*

Several classes of materials manifest displacive phase transitions, including shape memory alloys, many electronically correlated materials, superconductors, and ferroelectrics. Each of these classes of materials displays a wide range of fascinating properties and functionalities that are studied in disparate communities. However, these materials' classes share similar electronic and phononic instabilities in conjunction with microstructural features. Specifically, the common motifs include twinned microstructures, anomalies in the transport behavior, softening of specific phonons, and frequently also (giant) Kohn anomalies, soft phonons, and/or nesting of the Fermi surface. These effects, phenomena, and their applications have until now been discussed in separate communities, which is a missed opportunity. In this perspective a unified framework is presented to understand these materials, by identifying similarities, defining a unified phenomenological description of displacive phase transitions and the associated order parameters, and introducing the main symmetry-breaking mechanisms. This unified framework aims to bring together experimental and theoretical know-how and methodologies across disciplines to enable unraveling hitherto missing important mechanistic understanding about the phase transitions in (magnetic) shape memory alloys, superconductors and correlated materials, and ferroelectrics. Connecting structural and electronic phenomena and microstructure to functional properties may offer so-far unknown pathways to innovate applications based on these materials.

1. Introduction

Displacive phase transitions, (see **Table 1** and (**Figure 1**))—often also called martensitic phase transitions—occur across a wide range of materials: i) they determine the function of a material in application-relevant shape memory alloys and ferroelectric and piezoelectric materials; ii) they determine the formation of charge density waves (CDW) and spin density waves (SDW); iii) they are closely related to Verwey and Mott-insulator transitions; iv) the electronic nematic phase forms at a displacive phase transition.

Because of their wide manifestations, displacive phase transitions are important for several materials science communities. Yet, despite the shared importance of displacive phase transitions across communities, there is little to no cross-talk between the disciplines. This is a missed opportunity because mechanistic insights, experimental techniques, and theoretical frameworks are not shared between the disparate communities, thus

A. Grünebohm, R. Drautz
Interdisciplinary Centre for Advanced Materials Simulation (ICAMS) and
Center for Interface-Dominated High Performance Materials (ZGH)
Ruhr-University Bochum
Universitätsstr. 150, 44801 Bochum, Germany

A. Hütten, I. Ennen, L. Caron, T. Kuschel, D. Anselmetti, T. Dahm,
G. Schierning
Department of Physics
Bielefeld University
Universitätsstr. 25, 33615 Bielefeld, Germany
E-mail: gschierning@physik.uni-bielefeld.de

A. E. Böhmer, I. Eremin, F. Lechermann
Faculty of Physics and Astronomy
Ruhr-University Bochum
Universitätsstr. 150, 44801 Bochum, Germany

A. E. Böhmer, F. Weber
Institute for Quantum Materials and Technologies
Karlsruhe Institute of Technology
76021 Karlsruhe, Germany

 The ORCID identification number(s) for the author(s) of this article can be found under <https://doi.org/10.1002/aenm.202300754>

© 2023 The Authors. Advanced Energy Materials published by Wiley-VCH GmbH. This is an open access article under the terms of the Creative Commons Attribution-NonCommercial-NoDerivs License, which permits use and distribution in any medium, provided the original work is properly cited, the use is non-commercial and no modifications or adaptations are made.

DOI: 10.1002/aenm.202300754

Table 1. Displacive phase transitions.

Displacive phase transitions are non-diffusive phase transitions that occur with short-range shift of atoms. The characteristic structural changes occur by coordinated and homogenous displacements of atoms relative to their next neighbors within one unit cell. Because these displacements are small in relation to the interatomic distance, all atoms maintain their relative relationship. In materials science, the most famous phase transition of this kind occurs in the Fe-C system. Upon the phase transition, the high temperature perfect Fe cubes transform into distorted cubes by the incorporation of interstitial C. The high-temperature high-symmetry phase is called austenite, the low-temperature low-symmetry phase is called martensite, defining as another term martensitic phase transition for this displacive phase transition. Because of the coordinated movement of atoms, sometimes also the term military phase transition can be found. The terms displacive, martensitic, and military phase transition all describe the identical phenomenon, but are used in different communities. Such phase transitions are commonly characterized by frozen in phonon modes, such as shear or shuffle or relative shift of atoms as depicted in Figure 1.

giving rise to fractured and incomplete understanding of these fundamental phenomena.

Through this perspective, we aim to rectify this issue by identifying common motifs across disparate material classes to provide a unified understanding of how displacive phase transitions emerge therein and connect different communities around a common framework to study and harness these phenomena. For example, in the field of 2D and electronically correlated materials, there have been tremendous methodological developments to characterize in detail electronic and phononic instabilities and disentangle their contributions. These state-of-the-art methods have not yet been applied to the same extent on classical engineering materials, although similar effects are present also in these materials. As we argue in this perspective, sharing this methodological know-how across the disciplinary boundaries will open up significant research opportunities. Similar crossdisciplinary

J. Frenzel
Institute for Materials
Faculty of Mechanical Engineering
Ruhr-University Bochum
Universitätsstr. 150, 44801 Bochum, Germany

K. Rosnagel
Institut für Experimentelle und Angewandte Physik
Christian-Albrechts-Universität zu Kiel
24098 Kiel, Germany

K. Rosnagel
Ruprecht Haensel-Labor
Deutsches Elektronen-Synchrotron DESY
22607 Hamburg, Germany

G. Schierning
Research Center Future Energy Materials and System (RC FEMS)
Research Alliance Ruhr
University of Duisburg-Essen
47057 Duisburg, Germany

G. Schierning
Center for Nanointegration Duisburg-Essen (CENIDE)
University of Duisburg-Essen
47057 Duisburg, Germany

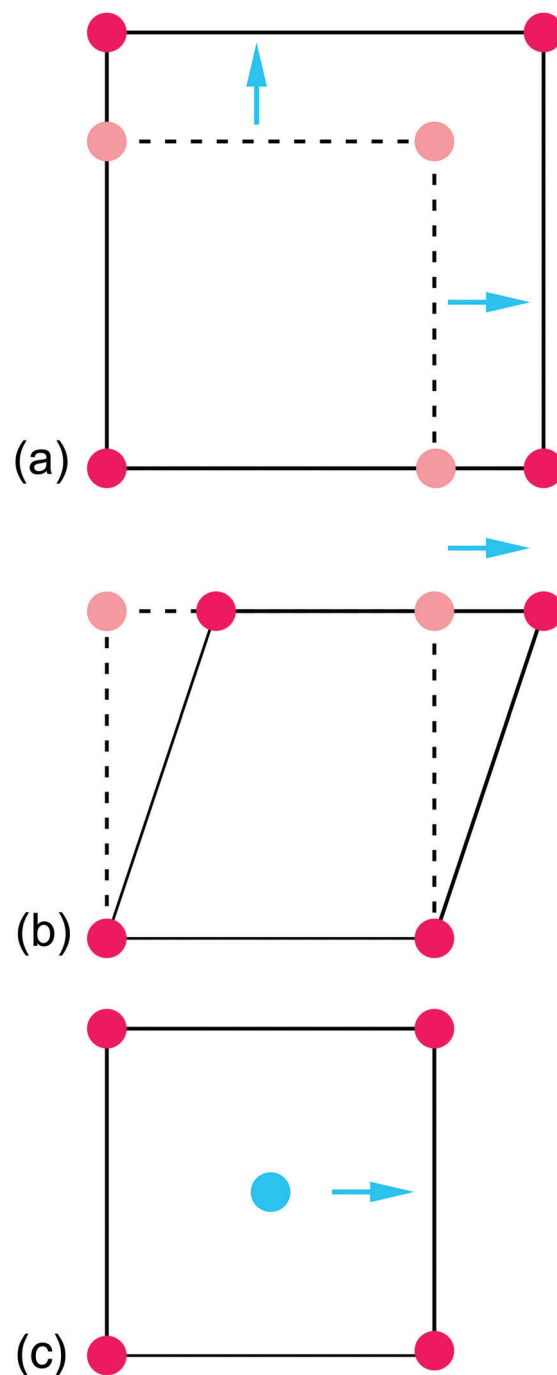


Figure 1. Displacive phase transitions by a) volume changes; b) shearing; c) atomic displacements.

added-value can be obtained by bringing the extensive insight that exists in the engineering disciplines about the influence of microstructure on displacive phase transitions, also to solid-state physics, where such studies are underrepresented. Crucially, bringing together the disparate communities around a unified framework by identifying common phenomena and mechanisms would enable filling many “white spots” in fundamental mechanistic understanding, which would in turn enable to deter-

ministically control displacive phase transitions (in terms of effect strength, reversibility, or application temperatures) to achieve desired properties and function of different materials' classes in applications.

We have organized the perspective as follows: In Section 2 we identify common microstructural, electronic, and phononic signatures in displacive phase transitions in important representative materials from the materials' classes. In Section 3, we analyze the fundamentals of displacive phase transitions to unite the standard interpretations (i.e., statistical physics and quantum phases, and materials science and the classical treatment of the martensitic phase transition) and review the symmetry-breaking effects and electronic phenomena that commonly occur at such transitions. In Section 4, we discuss important applications of materials exhibiting such phase transitions—shape memory alloys, superconductors, and ferroelectric materials. We bring all these insights together in Section 5, where we present research opportunities and perspectives arising from the interdisciplinary, unified framework presented in this perspective, before offering concluding remarks in Section 6.

2. Common Motifs

Displacive phase transitions govern functional properties that are utilized and/or occur in shape memory alloys, many electronically correlated materials and superconductors, and ferroelectrics. In the latter case, the superconducting phase is intertwined with either CDW or SDW or a nematic phase transition. The phase transitions themselves, though utilized and experimentally characterized in different ways in these different communities, share many similarities. Therefore, in the following sections, this perspective analyses the regularly occurring motifs of these displacive phase transitions and discusses their commonalities with regard to the microstructural, electronic, and phononic signatures.

2.1. Microstructural Signatures

One striking commonality of displacive phase transitions is the typical microstructural signature of the low temperature phase, the so-called martensitic texture, with its hierarchically twinned structures covering all length scales. Within this section, we will explain how the hierarchically twinned structures develop and give examples of such martensitic textures in shape memory alloys, superconductors, and ferroelectrics.

The crystal structure of the low temperature phase has a lower symmetry than the high-temperature parent phase. Different crystallographic variants may form during the transition. Their peculiar ordering and the formation of interfaces in the typical martensitic microstructure depend on the interface of martensitic and austenitic phases. In case of ferroelectric materials also the term heterophase has been coined.^[1–4] It is meanwhile widely accepted that this peculiar microstructure originates from the transformation that basically represents a shear along a specific crystallographic plane, referred to as the habit plane,^[5] on which the atoms move over distances that are smaller than the lattice constants. Displacive phase transitions take place via nucleation,

growth, and movement of phase fronts through the material in the form of discrete avalanches.^[6]

To describe the martensitic microstructure a common phenomenological theory was developed by Wechsler and Bowles,^[5,12–14] and applied further to ferroelectric materials.^[1,14] This concept assumes that all stress occurring during the austenite-to-martensite phase transition is concentrated at the interface between the two phases and minimized by the formation of twin boundaries in the martensite. Note that the stress at ferroelectric phase boundaries and martensitic phase transitions of relevant superconductors like A15-type, cuprate- or iron-based superconductors is typically order(s) of magnitude smaller than in shape memory alloys, but still enough to define the microstructure.

A hierarchical model to classify the encountered structures in martensitic Ni₂MnGa thin films according to their length scales ranging from atomic to macroscopic structures was described by Kaufmann, Niemann, and Schwabe.^[9,10,15] It is summarized in the illustration in **Figure 2**. Starting from a cubic-to-tetragonal transformation, at which one of the cubic axes is stretched while the other two are compressed, three different martensite variants can occur (**Figure 2a**). The interface between two energetically equivalent martensite variants is known as (nano) twin boundary and represents the first level of the hierarchy. A nice example of the nano twinning process has been presented by Waitz in a NiTi shape memory alloy and can be seen in **Figure 2b**.^[7] A second interface, which is important for the formation of martensite texture, is the habit plane between the martensite and austenite phases. Due to a mismatch in length between the austenite and martensite cells the habit planes are not infinitely sharp. To minimize the elastic energy of this interface, the martensite reverses the order of variants in a modulated manner. The required new parallel twin boundaries for this arrangement are energetically favorable. The illustration in **Figure 2c** shows exemplarily a monoclinic modulation of the martensite. This periodic arrangement of fine parallel martensitic twins can often be observed in NiMn-based magnetic shape memory Heusler compounds.^[16,17]

Niemann et al. determined elongated diamonds as a general shape of martensitic nuclei in Ni₂MnGa films (**Figure 2f**), which can grow to a parallelepiped of nuclei keeping the same interface orientations.^[9] The shape of the diamond nucleus can be divided by three mirror planes (**Figure 2e**). Therefore, up to eight units each consisting again of martensitic twins can be enclosed in the nuclei. A parallel coalescence of these martensite nuclei, linked by mesoscopic twin boundaries at the mirror planes, can form larger structures which are known as superdomains or metodomains.^[18] One of the most common patterns is the herringbone structure (**Figure 2g**). This is also widely observed in ferroelectric crystals like BaTiO₃ and can be seen in **Figure 2h**.^[11,19] Moreover, it has been reported in superconducting materials such as YBa₂Cu₃O₇,^[20,21] and twinned domain structures were also observed in FeSe single crystals below their nematic phase transition.^[22] The last step in this hierarchical order is the arrangement of several differently oriented herringbone structures with macroscopic twin boundaries in between.

In summary, a multiple twinned microstructure, often with hierarchical structure, is a fundamental common feature of this interesting class of functional materials. This microstructural signature is of utmost importance and directly related to the

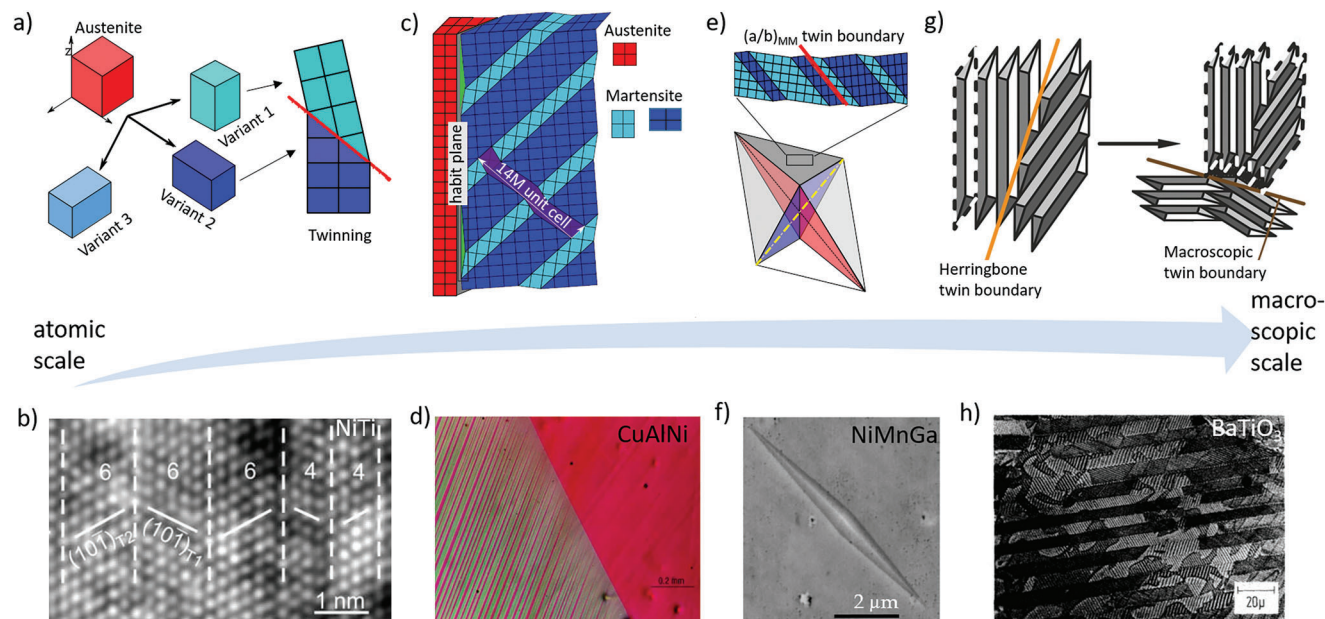


Figure 2. Formation of the typical martensitic microstructure at the displacive phase transition by a,c,e,g) schematic sketches and b,d,f,h) typical realizations from atomic scale (a and b) up to the hierarchical macroscopic structure (g and h). a,b) Three different martensitic variants may form at the transition, which can coexist on the atomistic scale and are separated by twin boundaries marked by red lines. Exemplarily, twin boundaries found by high resolution micrograph of NiTi; Reproduced with permission.^[7] Copyright 2008, Springer. c,d) Formation of adaptive martensite during the phase transition by the specific ordering of nano-sized twins: The stress at the interface between the austenite (red) and martensite (blue), that is, at the habit plane, can be released by the formation of nano-sized twins with specific stacking, for example, in the monoclinic structure whose unit cell is marked by the violet area. Corresponding fine laminate twin structure close to the habit plane in Cu-Al-Ni recorded by optical micrography; Reproduced with permission.^[8] Copyright 2005, Springer. Note that nanosized adaptive phases are also common for ferroelectrics and are also known as heterophases. e,f) The habit planes typically enclose martensitic nuclei with diamond shape as observed in the 5 μm thick Ni₂MnGa film; Reproduced with permission.^[9] Copyright 2017, Elsevier g,h) A parallel arrangement of nuclei (diamonds and parallelogram shaped) results in a herringbone pattern in the martensitic phase. This structure can grow up to the macroscopic scale by coalescence with further herringbone laminates; Reproduced with permission.^[10] Copyright 2021, John Wiley. h) Micrograph of a herringbone pattern observed in a BaTiO₃ crystal; Reproduced with permission.^[11] Copyright 1980, American Institute of Physics.

functionality, for example, in shape memory alloys, for which it is thus also intensively studied. Also, in ferroelectric materials, the twinned microstructure indirectly impacts the functionality and is therefore well investigated, while for electronically correlated materials showing displacive phase transitions the focus of research is so far more often on “untwinned” or “detwinned” materials.

2.2. Electronic Signatures

Electronic signatures of the displacive phase transition occur in a wide range of materials. Together with the reduction in symmetry at the phase transition the bonding situation in the materials changes. This necessarily changes the electronic properties. Electrical transport is one representative electronic property, and transport anomalies usually occur at displacive phase transitions. These anomalies, on the first glance, have their own characteristic fingerprint in the temperature-dependent resistivity ρ , but at second glance the underlying mechanism is similar. The characteristic shape of ρ may exhibit a steep increase, characteristic of a metal-insulator transition; a maximum, or just a small kink if the martensitic phase remains metallic. However, as will be shown,

the common feature is the reduction in charge carrier concentration, which contributes to the transport from the austenitic to the martensitic phase, accompanied by an increase in carrier mobility.

Figure 3 shows a compilation of transport data for different materials at the respective displacive phase transition. These are VO₂,^[23] NbSe₃,^[24,25] FeSe,^[26,27] and Ni₅₀Ti₅₀^[28] as prototypic representatives for a Mott metal-to-insulator transition, a CDW phase transition, a nematic phase transition in an unconventional superconductor, and a shape memory alloy phase transition, respectively.

The transport anomalies shown in Figure 3 are a steep increase of ρ at the metal-insulator transition of VO₂, a distinct bump or “nose-like” maximum in NbSe₃, a small upward visible kink in FeSe, and a small maximum in Ni₅₀Ti₅₀. Looking in more depth into the change of the transport properties at the phase transition reveals that ρ is actually not a good measure to describe the transport anomaly. What is more insightful is to look at the change of the mobility μ and the carrier density n upon the phase transition. For all prototypic materials discussed here, a decrease of the carrier density n was found at the displacive phase transition. The order of magnitude of this reduction varies. With several orders of magnitudes, the reduction of n is the strongest for the

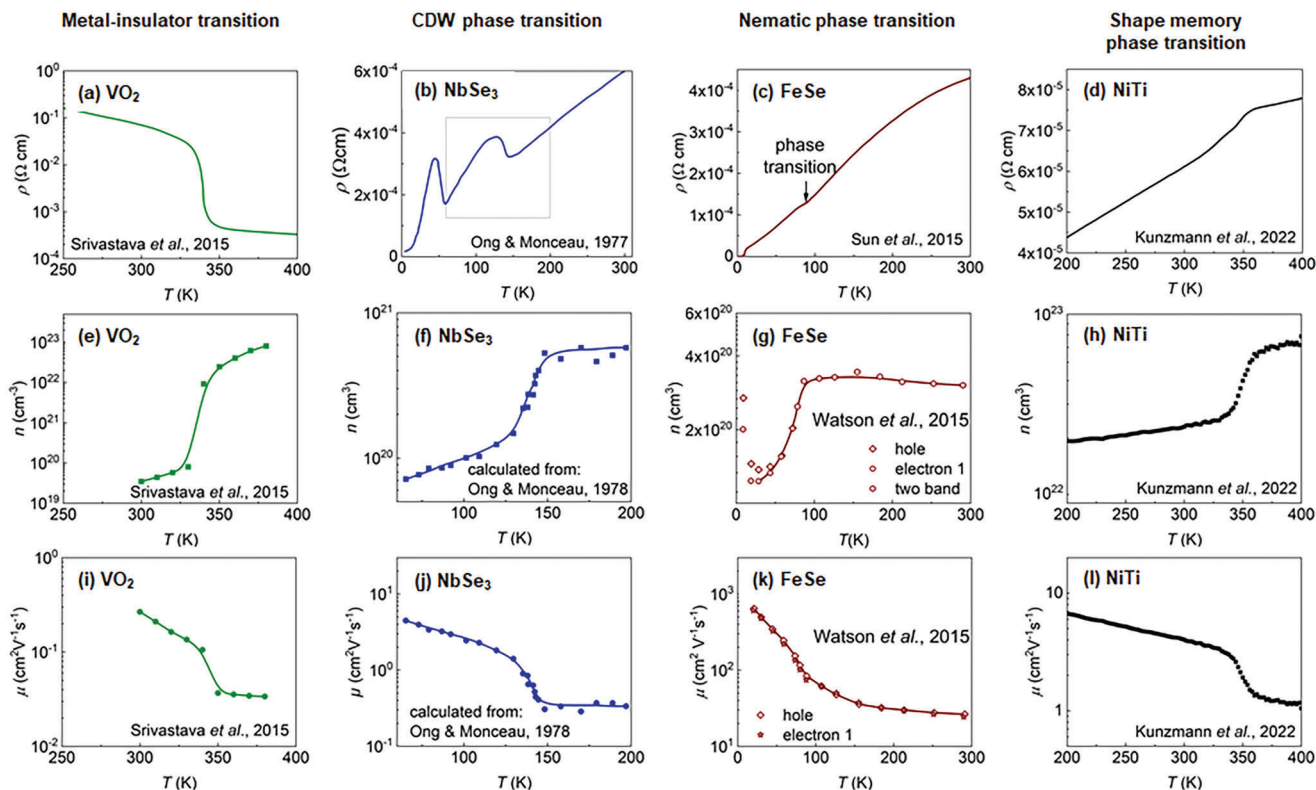


Figure 3. Transport anomalies at martensitic phase transitions in prototypic example materials of different material families. These are VO₂ (Data from the following sources: VO₂: 60 nm epitaxial, single phase thin film on (001)SrTiO₃(STO) substrates fabricated by pulsed laser deposition. The Hall data evaluation by a single band model from Ref. [23]. Srivastava, A., et al., Selective growth of single phase VO₂ (A, B, and M) polymorph thin films. *APL Materials*, 2015. 3(2): p. 026101, 23. Ibid.), NbSe₃ (NbSe₃: high quality single crystals. Resistivity data obtained from Ref. [25]. Ong, N.P. and P. Monceau, Anomalous transport properties of a linear-chain metal: NbSe₃. *Physical Review B*, 1977. 16(8): p. 3443-3455., original Hall data, R_H, published in Ref. [24]. Ong, N.P. and P. Monceau, Hall effect of a linear-chain metal: NbSe₃. *Solid State Communications*, 1978. 26(8): p. 487-491. Note that at 15 K, R_H evidences a zero-crossing, hence a transition from n-type to p-type behavior. Consequently, a multiband model would be necessary to calculate the quantities *n* and *μ* from the R_H, as discussed in Ref. [24]. Ibid. Therefore, these quantities were not provided in the original paper. For the sake of a representation within this review, R_H was used in combination with a single band model ($R_H = \frac{1}{en}$), but only in the temperature range from 60 to 200 K, hence well above the zero-crossing of equal charge carrier densities for n-type and p-type carriers. In this temperature regime, a low R_H points toward a high n-type charge carrier density, so that a dominance of these n-type charge carriers seems plausible, neglecting the influence of the p-type charge carriers. *μ* was calculated using a single band Drude model from *ρ* and R_H), FeSe (FeSe: high quality single crystals. Resistivity data taken from Ref. [26]. Sun, Y., et al., Critical current density, vortex dynamics, and phase diagram of single-crystal FeSe. *Physical Review B*, 2015. 92(14): p. 144509., Hall data from Ref. [27]. Watson, M.D., et al., Dichotomy between the Hole and Electron Behavior in Multiband Superconductor FeSe Probed by Ultrahigh Magnetic Fields. *Physical Review Letters*, 2015. 115(2): p. 027006. The Hall data evaluation by employing a multiband model, including two electron pockets and one hole pocket. Hereby, the electrons from one pocket, labeled electron 2 in Ref. [27]. Ibid., have an approximately one order of magnitude lower *n* than the electrons of type electron 1. For simplification of the representation, the *n* and *μ* data of carriers of the type electron 2 are not shown here, since their absolute quantity is outnumbered by carriers of the type electron 1.), and Ni₅₀Ti₅₀ (Ni₅₀Ti₅₀: polycrystalline sample of stoichiometric composition Ni₅₀Ti₅₀ for resistivity and Hall characterization from Ref. [28]. Kunzmann, A., et al., The role of electrons during the martensitic phase transformation in NiTi-based shape memory alloys. *Materials Today Physics*, 2022: p. 100671. Hall data evaluation was done using a single band model.) as examples for a metal-insulator transition, a CDW phase transition, a nematic phase transition of a superconductor, and a shape memory alloy phase transition. Panels (a–d) show the resistivity, panels (e–h) the charge carrier density, and panels (i–l) the Hall-mobility of the respective materials VO₂, NbSe₃, FeSe, and NiTi. While the resistance anomalies at the phase transition differ from material to material, they all show a distinct decrease in carrier density, accompanied by an increase in carrier mobility at the phase transition.

metal-insulator transition in VO₂. For all other shown materials, the decrease of *n* remains within approximately one order of magnitude. The charge carrier mobility *μ* shows an opposite trend in all cases and increases at the phase transition. As a result, these similarities in the development of *n* and *μ* between these otherwise quite different materials point toward related changes of atomic bonding and electronic structure at the displacive phase transitions. Whenever the electronic density close to the Fermi

level is reduced, the charge density will be reduced—either by a full opening of a gap in case of the metal-to-insulator transition or to a smaller extent by pseudogaps. The extent of this reduction will depend on material specific parameters and on the specific underlying mechanism. The change of the carrier mobility *μ* may hint at modified charge carrier scattering, for example, by different electron-phonon (e–ph) coupling, but remains poorly understood. Additionally, the changing character of the bonding

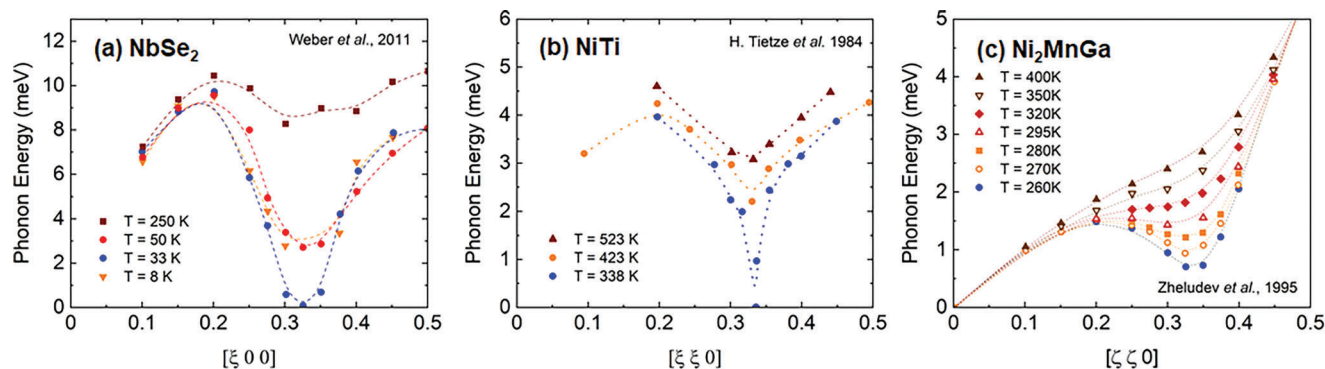


Figure 4. Softening of acoustic phonon modes in a) the CDW material NbSe₂, in b) the shape memory alloys NiTi, and in c) the magnetic shape memory alloy Ni₂MnGa. Measured phonon dispersion for different temperatures a) along $[\xi 0 0]$ in NbSe₂ (Adapted with permission.^[29] Copyright 2011, American Physical Society.), b) along $[\xi \xi 0]$ in NiTi (Adapted with permission.^[30] Copyright 1984, Institute of Physics.), c) along $[\xi \xi 0]$ in Ni₂MnGa (Adapted with permission.^[31] Copyright 1995, American Physical Society.).

corresponds to a decrease in the electrons' degrees of freedom, hence a reduction of the entropy of the subsystem of electrons, as discussed for NiTi.^[28]

It thus seems that the reduction of the charge carrier concentration at the displacive phase transition is a common motif of these transitions, at least in the case of metals. The charge carriers that contribute to the transport are found in the conduction bands possessing a high kinetic energy. A reduction of the number of electrons in the conduction bands can therefore be energetically favorable.

2.3. Phononic Signatures

The third signature common to displacive phase transitions is a softening of phonon modes that occurs if the austenitic phase is cooled toward the martensitic phase. Softening of phonon modes hereby means that a particular phonon mode at a particular wave vector decreases in energy—that is, becomes softer. Softening is necessary to allow the atoms to move. The extent of this phonon softening as well as the particular wave vector involved varies in different materials, which in turn raises the question on the driving mechanism of the displacive phase transition. This is in our opinion still not fully understood. Sometimes, the specific phonon mode just flattens a little, sometimes distinct anomalies in the phonon dispersion relation can be found. In some cases, this phonon mode may reach zero at the phase transition and atoms can move freely according to the soft mode's vibrational pattern. The dynamical vibration “freezes” into a static displacement pattern of the atoms, resulting in a new/distorted lattice structure.

A complete softening of a phonon mode would be expected for structural phase transitions. In fact, it is surprising that there are so many subtle differences in the soft-mode properties: full softening with sharp/broad dispersion, incomplete softening with a central peak, no softening but strong damping, etc. While softening is found to a greater or lesser extent in all displacive phase transitions, beyond this, similarities in the phonon dispersion relations of different materials provide the opportunity to interpret mechanistically the driving forces of phase transitions. From this

viewpoint, it is noteworthy that the phononic signatures in different materials, for example, NiTi shape memory alloy, Ni₂MnGa magnetic shape memory alloy, and the CDW material NbSe₂ show extremely similar features. **Figure 4a** shows examples of phonon softening in the well-known CDW material NbSe₂ from ref. [29]. When the temperature is decreased toward the transition temperature of $T_{\text{CDW}} = 33$ K, the frequency of a specific phonon mode goes down and reaches zero at the phase transition temperature, T_{CDW} . Interestingly, analogous phonon softening is seen in NiTi^[30] and Ni₂MnGa,^[31,32] for example, as shown in Figure 4b,c.

Regardless of the specific underlying physical mechanisms it can be noted that the tremendous similarity of the signatures in the phonon dispersion of two extremely well-studied shape memory alloys and a prototypical CDW material is striking. This suggests that these shape memory alloys may belong to the class of materials, for which electronic degrees of freedom are strongly involved in determining the displacive phase transition. This requires further analysis.

3. Fundamentals of Displacive Phase Transitions

The strong similarity of microstructural, electronic, and phononic signatures in quite different classes of materials exhibiting displacive phase transitions asks for a unified description of these transitions and their driving forces.

One important hypothesis for temperature driven displacive structural phase transitions is that the high-temperature, high-entropy austenitic phase (A) has a higher symmetry than the low-temperature, low-entropy martensitic phase (M). To define a signature of the phase transition and measure its degree, it is convenient to define a set of order parameters Φ_i . Here the displacements themselves are obvious choices of order parameters. These may include homogeneous changes of the strain tensor and the shift of atoms against each other. These displacements always change the bonding character and thus the electronic structure and transport properties.

Electronic order parameters may have a complex internal structure and depend on the particular material class. The order parameter(s) Φ_i of the phase transition are given by the mean value(s) of the underlying microscopic variables, for example, the

magnetization M is related to the local moments as $M = \langle M_i \rangle$ ^[34] and the order parameters are first moments of the distribution functions, for example, of M_i . They give insight into the degree of the specific ordering but do not give a direct answer on the underlying driving forces, especially if one can define more than one Φ_i and if several parameters are coupled. To disentangle electronic and structural driving forces the corresponding susceptibilities are needed. For instance, the magnetic or dielectric susceptibilities can be directly measured in an external electric or magnetic field, Knight-shift and spin-lattice relaxation in nuclear magnetic resonance (NMR) and nuclear quadrupole resonance (NQR), spin-structure factor in neutron scattering. In cases of order parameters such as nematic, orbital, or elastic strain, addressing susceptibilities is an even more challenging experimental task.

Further important measures are cross-susceptibilities like the pair correlation $\langle \Delta r_i \cdot M_i \rangle$ between the displacements Δr_i and the local magnetization M_i . They correspond to higher-order moments of distributions. Correlations change at the phase transitions but are not necessarily primary-order parameters for the transition. For a full characterization of the phase transition, it is thus needed to record the evolution of the complete set of order parameters, the related susceptibilities, and correlations. If possible, the detection of one susceptibility for fixed other order parameters allows to distinguish between driving forces and secondary effects. Furthermore, electronic and structural degrees of freedom may be disentangled in the time-domain.

The displacive phase transitions discussed in this perspective are transitions between competing phases that have compatible atomic structures and enable diffusionless atomic rearrangements. So, there must be a simple path between austenite and martensite, which converts the phases into each other such as the Bain path. At the transition temperature there are two possibilities how the path can be followed, see **Table 2**.

Either, the free energy along the path decreases monotonically with temperature, resulting in a continuous second-order phase transition. This transition can spontaneously be induced by thermal fluctuations (thermal transition). Or, there is an energy barrier in the free energy, so that the path is not continuously traversed, but only when the difference in the free energy becomes large enough. This corresponds to a first-order phase transition with thermal hysteresis and latent heat. Typically, diffusionless phase transitions are called weak first-order transitions as they show a smaller jump of the macroscopic thermodynamic quantities (e.g., the order parameter) than the typical first-order phase transition. In addition, thermal fluctuations which usually drive second-order phase transitions can also not be neglected near weak first-order phase transitions. Particularly, for the order parameter monitoring the tetragonal distortion at the cubic to tetragonal phase transition, the free energy is not symmetric with respect to inversion resulting in odd terms (see **Table 2**).

Alternatively, the energy landscape as obtained in atomistic modeling may include higher order terms. Without stringent mathematical derivation, the $C\Phi^6$ -term allows to account for the energy barrier between both phases, for example, the interface energy of the moving phase boundary of the nucle-

ation. In this case, elastic (and electrostatic) matching of both phases can be used to systematically reduce the signatures of the first-order phase transition, for example, the hysteresis.^[35] The other way around, if a second-order character of the transition is expected for the primary order parameter by symmetry, (linear) coupling between structural and electronic order parameters breaking the same symmetry or between the primary (incipient) instability and shear strain add odd terms to the energy expansion. Among others, this results in a temperature-dependent renormalization of the coefficients and may induce a finite energy barrier and a first-order character of the transition.

One of the most important signatures of a displacive phase transition is the softening of phonon modes, see **Section 2.3**. Phonon softening means that a particular phonon mode $\omega_n(q)$ at a particular wave vector decreases in energy, that is, becomes softer if the system approaches the phase transition. This may include modes with $q \rightarrow 0$ (elastic moduli), zone boundary modes (ferroelectric and antiferroelectric transitions), or modes within the Brillouin zone.

In the Landau picture, this softening is given as $A = a(T/T_c - 1) = m^*\omega^2$, with m^* and ω , the effective mass and the frequency of the related phonon mode. In the ideal case of a second-order transition, see **Table 2**, this frequency decreases until it reaches zero at the phase transition. This means that the dynamical vibrations become “frozen” and create a static displacement pattern of the atoms with a wavelength and direction given by the eigenvector of the phonon, resulting in the new lattice structure. While the total energy of the system is reduced by the freezing of the soft mode, the stability of both phases is given by the free energy and thus the entropy, particularly the phonon contribution, which stabilizes the high temperature phase above T_c . It is commonly accepted that the softening of the phonon modes beyond thermal expansion indicates an intrinsic instability of the lattice toward a second-order phase transition. However, it has been reported early that a pure change of cell shape only allows for second-order transitions in specific symmetries, such as tetragonal to orthorhombic but not cubic to tetragonal.^[33]

Furthermore, the soft mode picture is in stark contrast to the weak first-order character of displacive phase transitions and the simultaneous softening of phonons upon displacive phase transitions calls for its understanding. Note that softening is often observed as precursor of the displacive phase transitions.^[36] Interestingly, the displacement across the phase transition does not necessarily coincide with the soft mode (q point and eigenvector) of the high temperature phase. Whether this is caused by phonon-phonon interactions or the interaction with another (electronic) order is a complex question that needs to be solved for each material system.

The most common theoretical approach to access phonon spectra, characterize soft phonon modes and analyze their coupling to other degrees of freedom is density functional theory (DFT).^[37–46] Important breakthroughs in the last years also include the design of new phases by substitution and strain by screening and analysis of soft modes. Important challenges are the treatment of microstructure and thermal excitations. Advanced approaches now allow to directly access the renormalization of phonons by anharmonic effects and the temperature dependency of soft phonon modes, see for example.^[47–58]

Table 2. Classification of displacive phase transitions by their order.

Second-order phase transition	<p>Second-order structural phase transitions are continuous transitions of the order parameter(s) without an energy barrier. They can be described by a Landau free energy $F(\Phi) = A\Phi^2 + B\Phi^4$. Thereby, a temperature-dependent coefficient $A = a(T/T_c - 1)$ results in the typical Curie–Weiss-like change of the order parameter. In the soft mode picture the phase transition is driven by the freezing of a particular phonon mode at a specific q at the critical temperature T_c, that is, $\omega(q) = 0$. However, it has been reported that a pure change of cell shape only allows for second-order transitions in specific symmetries, such as tetragonal to orthorhombic but not cubic-to-tetragonal.^[33]</p>		<p>Phenomenological pictures of the evolution of the free energy across the transition temperature T_c depending on an order parameter Φ. In the soft-mode picture ω is the frequency of the soft phonon mode reaching 0 at the transition.</p>
(Weak) first-order phase transition	<p>First-order transitions are abrupt phase transitions with thermal hysteresis and an energy barrier between both phases (latent heat). Weak first-order phase transitions can be described by a Landau free energy if terms with odd symmetry occur, $F(\Phi) = A\Phi^2 + C\Phi^3$, or higher order potential terms like $F(\Phi) = A\Phi^2 + B\Phi^4 + C\Phi^6$. Softening of the phonon mode(s) may be a precursor of the transition but commonly $\omega(q) > 0$ for all temperatures.</p>		<p>Phenomenological pictures of the evolution of the free energy across the transition temperature T_c depending on an order parameter Φ for a weak first-order transition. At the transition temperature, the high and low-temperature phases are degenerated and separated by an energy barrier.</p>
Coupling of primary order parameters	<p>Second-order phase transitions can become weakly first-order by the coupling of the primary-order parameter Φ with at least one secondary-order parameter Φ_2 which breaks the same symmetry as Φ. Weak first-order phase transitions can become again second-order by a systematic reduction of the energy barrier, for example, by elastic matching of both phases or precursor phases. Note that it is sometimes an experimental challenge to distinguish weak first-order phase transitions from second-order phase transitions due to limited resolution of the data and inhomogeneity in the samples.</p>		<p>Phenomenological picture of the change of the energy barrier of a weak first-order phase transition, for example, by elastic matching.</p>

3.1. Brief Overview of Symmetry Breaking Effects and Electronic Driving Forces

Electronic driving forces are often associated with changes in the electronic structure during the phase transition. However, the separation into elastic and electronic contributions to phase transitions is not a straight forward task. One has to distinguish between cooperative electronic and structural driving forces and

pure electronic driving forces. Many models, for example, DFT, use the Born-Oppenheimer approach and minimize the combined electronic and atomistic degrees of freedom with respect to the electronic degrees of freedom. The resulting free energy depends only on atomic degrees of freedom. This means fluctuations in the electronic system are disregarded. If a phase transition takes place in such a model it thus also has to be a structural phase transition in which electronic degrees of freedom play a

secondary role. However, they can still change the character of the transition from second-order to (weak) first-order by the discussed linear coupling.

The common symmetry-breaking effects and instabilities that occur at displacive phase transitions are briefly described in **Table 3**. From a historical point of view, the Verwey metal-to-insulator transition was the first to be described.^[59,60] It is based on charge ordering which is a common motif in many displacive phase transitions. A little later, the Mott metal-to-insulator transition^[61] and the Peierls metal-to-insulator transition were postulated.^[62] The Mott metal-to-insulator transition is found in strongly correlated materials, historically interpreted as a purely electronic effect, but often found in combination with a structural transition.^[63]

In metals, Fermi surface nesting is often considered to play a pivotal role as origin of electronic instabilities. A Fermi surface is nested if large sections (or all) of it can be connected by a single wave vector q . For instance, the Peierls metal-to-insulator transition, originally proposed for a metallic 1D chain of atoms,^[62] is driven by an instability in the electronic system due to perfect nesting of two Fermi points, and results in the formation of a CDW. When e–ph coupling (EPC) is finite, this transition is accompanied by phonon softening at the nesting wave vector $q_{\text{CDW}} = 2k_{\text{F}}$ (k_{F} is the Fermi wave vector). For a half-filled conduction band, $k_{\text{F}} = \pi/2a$ (lattice constant a) leads to a CDW wavelength of $2a$, that is, a doubling of the unit cell. While this scenario seems to apply for some quasi-1D compounds,^[64–66] it turned out that for CDW transitions in quasi-2D systems, in which the nesting of the Fermi surface can only be partial, the situation is less obvious. For example, it has recently been found that Fermi surface nesting alone fails to explain the CDW transition in the layered transition metal dichalcogenide NbSe₂ (ref. [29] and others). Instead, the momentum dependence of EPC was established to determine the characteristics of the CDW phase.^[67,68] The momentum-dependent EPC scenario differs from the Peierls mechanism in the primary driving force of the CDW transition. In the Peierls mechanism it is the Fermi surface nesting-driven instability of the electron system which causes the lattice distortion and the phonon softening leading to it. The momentum-dependent EPC, in contrast, drives a CDW transition by coupling certain phonons with certain wave vectors more strongly to the electrons than others,^[29,67,68] making the transition a combined electron-lattice instability rather than a (purely) electronically driven one.

With respect to the structural distortion—the dimerization—necessary to enable the phase transition, the Peierls instability and the Jahn–Teller effect, or pseudo-Jahn–Teller effect, are closely related. However, the latter may also occur in insulators. Here, it is not the kinetic energy of the free electrons that changes, but their electronic polarization. While the Jahn–Teller effect is restricted to degenerate atomic orbitals, also pseudo degenerate (close in energy) orbitals may allow for the pseudo or second-order Jahn–Teller effect. Phase transitions characterized by this kind of displacement are often called “martensite-like” and occur in oxidic perovskites with ABO₃ structure. During this transition, the covalency of the bonds changes as unoccupied t_{2g} orbitals on the B lattice site hybridize with oxygen molecular orbitals. The resulting first-order insulator-to-insulator transition is not only an elastic transition, but the atomic displacements cor-

respond to local dipole moments and result in the formation of ferroelectric and antiferroelectric phases.^[69,70]

When no phase transition occurs in the Born-Oppenheimer approach, electronic driving forces must be important. To go to this regime in atomistic modeling, additional constraints on the electronic structure have to be included (constraint DFT). As an interesting side effect of the separation of the electronic and atomic degrees of freedom in modeling, the temperature of the electronic system can be chosen differently from the temperature of the atomic system. This may be useful for comparing and contrasting temperature dependence in electronic and atomic contributions.

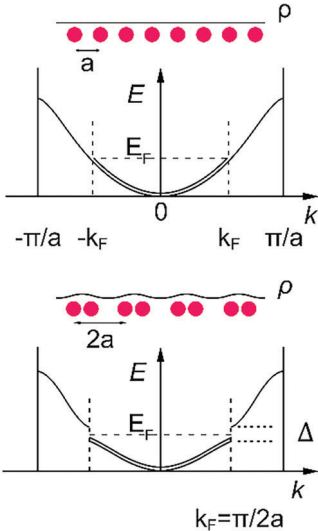
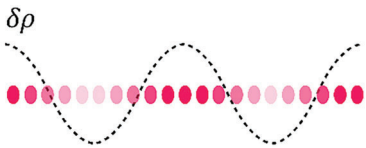
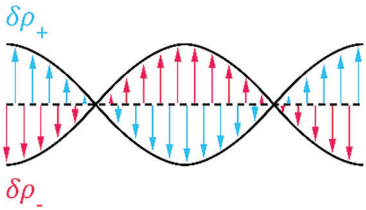
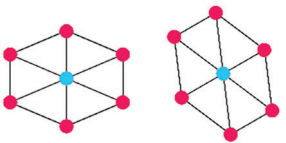
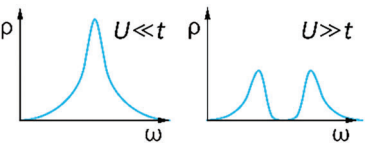
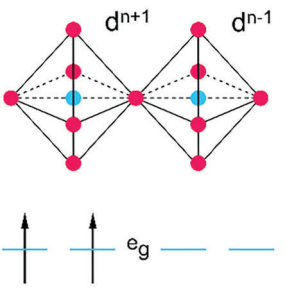
There is an (almost) universal understanding that a type of displacive phase transition has an electronic origin, namely, the so-called nematic phase transitions. Nematicity is defined here as rotational symmetry breaking via an electronic mechanism, which may occur in correlated metals, including several unconventional superconductors with the iron-based superconductors offering most prominent realization.^[71] Similar to the well-known case of a nematic liquid crystal, the spatial rotational symmetry is lowered (often from fourfold to twofold, that is, from a tetragonal to an orthorhombic symmetry) without breaking other symmetries so that the “nematic order parameter” is finite below the transition. In this picture, a simultaneous tetragonal-to-orthorhombic lattice distortion (typically in the order of a few %) is only a side-effect of the electronic transition.

The electronic mechanism of a nematic phase transition can be described as i) a Pomeranchuk instability of the Fermi surface, ii) the result of a (ferro)orbital instability that resembles the cooperative Jahn–Teller effect, or iii) a consequence of frustration in the magnetic correlations. The Pomeranchuk instability is an instability in the shape of the Fermi surface of a material with interacting fermions, causing deformations of the Fermi surface to be energetically favorable. Such an instability is enhanced when the electronic dispersion flattens near a particular symmetry point of the Brillouin Zone. In the (ferro)orbital instability scenario the conduction bands consist of degenerate orbitals at the high-symmetry points of the Brillouin zone in the tetragonal or cubic systems. Due to interaction, the degeneracy can be lifted, yielding a spontaneous (ferro)orbital order, which triggers in turn the tetragonal to orthorhombic phase transition. Finally, in the case of magnetic frustrations, the system splits into two antiferromagnetic sublattices whereas the relative orientation of one sublattice with respect to the other, necessary for establishing the long-range magnetic order, is not fixed. In such a case, the nematic order parameter, built out of the fluctuations of the magnetic order parameter, breaks the tetragonal symmetry of the lattice yielding the structural transition. Meanwhile, even though nematicity is evidenced in many materials, it is still considered a relatively exotic phenomenon.

Specific theoretical proposals for other electronic driving forces include but are not limited to magnetization, charge, and orbital density wave, spontaneous orbital current loops, Cooper-pairing, etc.

These effects can basically be divided into effects that occur in metals and those that occur in insulators, also defining the type of transition as metal-to-metal, metal-to-insulator, or insulator-to-insulator transition. While the metal-to-insulator and insulator-to-insulator transitions are known in this form,

Table 3. Instabilities and electronic effects at displacive phase transitions.

Peierls instability/Peierls transition	Electronic instability of a 1D metal chain at low temperatures with lattice parameter a , driven by Fermi surface nesting and associated with a periodic lattice distortion. The dimerization is accompanied by a spatially periodic modulation of the associated charge density, ρ (CDW)—and an opening of an energy gap Δ at the Fermi energy, E_F . A Peierls instability has a metal-to-insulator characteristic.	 <p>The diagram illustrates the Peierls instability in two states. The top part shows a 1D chain of atoms with lattice parameter a and a Fermi sea (red dots) at energy E_F. The corresponding band structure shows a parabolic band with Fermi points at $\pm k_F$. The bottom part shows the distorted chain with lattice parameter $2a$ and a charge density wave (CDW) modulation ρ. The band structure now has a gap Δ at the Fermi energy E_F, and the Fermi points are at $\pm k_F = \pm \pi/2a$.</p>
Charge density wave (CDW) transition	CDW transition due to momentum-dependent electron-phonon (e-ph) coupling (EPC) strength, which couples certain phonons with certain wave vectors more strongly to the electrons than others. This yields breaking of translational symmetry of the lattice with additional charge density modulation (CDW).	 <p>The diagram shows a chain of atoms with a dashed line representing the charge density modulation $\delta\rho$ superimposed on the lattice.</p>
Spin density wave (SDW) transition	Electronic transition driven by Fermi surface nesting resulting in spin density modulation (SDW).	 <p>The diagram shows a chain of atoms with spin density modulation $\delta\rho_+$ (upward arrows) and $\delta\rho_-$ (downward arrows) superimposed on the lattice.</p>
Electronic nematic transition	Electronically driven structural transition, which lowers the rotational symmetry of the system. No other symmetries are broken, so that only the “nematic order parameter” is finite below the transition. The origin of the electronic nematic order may be either a Pomeranchuk-type instability, (ferro)orbital order, or Ising nematic order in frustrated magnetic systems.	 <p>The diagram shows two different lattice structures: a high-symmetry structure on the left and a lower-symmetry nematic structure on the right.</p>
Mott transition	Metal-to-insulator transition due to local Coulomb repulsion often associated with a change in band width (due to a change in interatomic distance).	 <p>The diagram shows two plots of charge density ρ versus frequency ω. The left plot is for $U \ll t$ (metallic state) and the right plot is for $U \gg t$ (insulating state).</p>
Charge ordering and Verwey transition	Disorder-to-order transition with a metal-to-insulator characteristic. The transition from a dynamically disordered phase of polyvalent cations into a long range spatial ordering of the polyvalent cations that localizes the electrons and prevents hopping transport.	 <p>The diagram shows two lattice structures: a disordered phase on the left and an ordered phase on the right. Below the structures is a band structure diagram showing the e_g band.</p>

(Continued)

Table 3. (Continued).

Jahn–Teller effect	Lifting of the degeneracy of degenerate orbitals under tetragonal distortion results in the symmetry breaking Jahn–Teller effect.	
Pseudo-Jahn–Teller effect	Pseudo degenerate (close in energy) orbitals may allow for the Pseudo- or second-order Jahn–Teller effect.	
Tetrahedral/octahedral crystal field splitting	Lifting of the degeneracy of 3d-orbitals of transition metal atoms in tetrahedral or octahedral crystal fields. A transition between them causes the inversion of the involved energy levels.	

a metal-to-metal transition may best be described by the term “incomplete metal-to-insulator transition.” Here, the signature in electrical resistance remains small compared to a metal-to-insulator transition. This incomplete metal-to-insulator transition describes a transition, in which the density of quasi-particles at the Fermi level is reduced due to the partial gapping of the normal state Fermi surface. The opening of the charge gap is similar to the metal-to-insulator transition. However, the reduction of the charge carrier density remains at a level that one would not describe the low-temperature phase as an insulator (as, e.g., in NiTi), but rather as a metallic state, for which the charge carrier density is reduced and remaining charge carriers show higher mobility. These transitions cannot be simply understood in terms of a Peierls transition or Mott insulator transitions and are still the focus of the current research efforts.

4. Materials and Applications

The common motifs and related driving forces of displacive phase transitions link classes of materials that are usually investigated in disjunct communities. Therefore, in the following section, we highlight elemental metals, shape memory alloys, superconductors, and ferroelectrics as exemplary classes of materials harboring displacive phase transitions. We will hereby focus on electronic phenomena at this (function determining) phase transition.

4.1. Elemental Metals

Martensitic phase transitions occur in many elemental metals, most famously in Fe (with small amounts of C) and its alloys. In

fact, Fe-based materials in particular are the textbook example of martensitic phase transitions, and these transitions are often associated with complicated alloy compositions. CDW transitions, on the other hand, are often associated with the special properties of transition metals in their compounds. However, neither complicated alloy compositions nor the presence of elemental compounds is a prerequisite for either transition to occur. Therefore, when it comes to basic physical properties, it is helpful to turn to elemental metals, since the structural properties of monoatomic solids are usually better defined and also more accessible to theoretical studies.

Lithium (Li) is the lightest elemental metal and exhibits a martensitic phase transition that reduces the total energy of this primitive s-electron metal. However, although it appears to be a simple metal, the phase diagram of Li shows a richness of intermediate and high-pressure phases, that is far from being understood. As shown by neutron scattering techniques, Li transforms at a temperature of 74 K from body centered cubic (bcc) to a closed packed rhombohedral 9R structure, along a highly pressure-dependent transition path.^[72–75] This 9R structure has been considered the martensitic ground. Recently, by combining pressure-dependent synchrotron X-ray diffraction with multiscale simulations, it was shown that this 9R structure is only metastable and that a lower-energy face centered cubic (fcc) phase should be the ground state.^[76] This triggered an intense discussion and search for low-energy Li phases,^[77] with a bcc-to-fcc transition pathway proposed.^[78] To reach the fcc phase experimentally, pressure needs to be applied. Remarkably, Li exhibits the highest superconducting transition temperature of all elements at high pressures, with reports ranging from 9 to 16 K at 23 to 80 GPa^[79] to 20 K at 48 GPa.^[80] At such high pressures,

the occurrence of additional phases has been reported. For instance, at about 40 GPa, the fcc phase transforms, again via intermediate rhombohedral phases, into a cubic polymorph with 16 atoms per unit cell.^[81] This is consistent with the observation that the Li nuclei dimerize at sufficiently high pressures. The bcc structure is first destabilized to a Jahn–Teller mechanism, followed by a Peierls-type pairing distortion.^[82] This may be a prerequisite for a metal-to-insulator transition. While the Fermi surface shows no particular tendency to nest at normal pressure, extended nesting is observed with increasing pressure.^[83] Even though high-pressure Li shows such high superconducting transition temperatures, they are still much lower than the theoretical predictions.^[84] Therefore, the electronic causes of both the martensitic phase transformations in the rich phase diagram of Li and the electronic causes of the high-pressure superconductivity of Li are still an active and also controversially discussed research field.

Probably because sodium (Na) does not have the spectacular superconducting properties of Li, the scientific debate about its low-temperature phases is much less intense. However, one finds similar motifs and a not fully understood ground state. While the stable low-temperature phase is hexagonally closed packed (hcp),^[85] there is also evidence for the occurrence of a bcc-to-9R transition,^[86] and also the energy-barrier between the bcc and fcc phases is small.^[87] The martensitic phase transition in Na occurs at 35 K, but—depending on the report—into different low-temperature variants. The coexistence of long-range ordered close-packed hcp, 9R, and bcc sequences, whose relative volume fractions depend on temperature, has been reported,^[88] as well as a complex mixture of hexagonal and rhombohedral polytypes linked by stacking faults,^[89] but without fcc fractions in both studies.

The difference between the individual martensitic low-temperature phases of both, Li and Na, is of course relatively small—therefore stacking faults, which are abundant in these crystals due to their low formation energies, are now being discussed in connection with the occurrence of these phases,^[90] as potential external stimuli for these phase transitions. In line with this, a phenomenological model treats both the martensitic phase transitions in Li and Na^[91] and concludes that the complexity and richness of the low-temperature phase diagrams of Li and Na could be related to the particular special softness of their crystalline state, arguing in the same direction as the use of (easily formed) stacking faults.

As model systems, elemental metals, especially alkali metals, have played a notable role in the microscopic explanation of the CDW phase transition. This concerns in particular the view of the transition as a many-body instability in the exchange-correlation energy^[92] as well as the central role that electron-phonon coupling plays even in the idealized monoatomic chain.^[67] In practice, however, CDWs form very rarely in elemental systems.

The only pure elemental metal known to exhibit an original bulk CDW at ambient pressure is uranium (α -U). The CDW in α -U is 3D and characterized by a complex structural modulation and transition behavior.^[93] The CDW wavevector has three components. These are incommensurate with the underlying lattice at the transition into the CDW phase at 43 K, and all become commensurate in the course of two lock-in transitions at 37 and 22 K.^[94] In the normal phase, the phonon spectrum shows the

signatures of an incipient CDW; a Kohn anomaly at room temperature, and a softening of the corresponding phonon as the CDW transition temperature is approached.^[95,96] The results of first-principles calculations linked this behavior to a Peierls-like instability in which Fermi surface nesting of narrow f-electron bands may drive the transition in concert with momentum-dependent e-ph coupling.^[97,98] Electronic correlation effects due to the flat f-electron bands, which may also play a role in the CDW transition, have not been investigated.

In elemental systems other than α -U, CDWs can also occur, but not as original bulk phenomena at ambient pressure. In Cr, the incommensurate CDW appears as a by-product, that is, as the second harmonic of the fundamental spin-density (SDW) wave, which is thought to be driven by Fermi surface nesting.^[99] In the chalcogens S, Se, and Te and the halogens Br and I, CDW-type incommensurately modulated structures occur under pressure.^[100] And on the surfaces of elemental metals and semiconductors, CDWs can form, possibly favored by the dimensionality reduction from 3D to 2D or even 1D.^[101] Prominent examples are the pristine W(001) surface [Jupille94], ultrathin In films on Cu(001),^[102,104,105] ultrathin Pb and Sn films on Ge(111)^[103,104], and linear In chains on Si(111).^[105]

Despite these examples, CDWs in elemental systems remain an overall exception. Accordingly, the examples seem to show that the simple high-symmetry structures adopted by bulk elemental systems must first be made anisotropic in order to create a prerequisite for the formation of CDWs.

4.2. Shape Memory Alloys

In Section 2, we have seen two important findings that connect CDW phenomena and shape memory alloys. These were transport anomalies in NiTi that mimic those of electronically driven phase transitions in VO₂, NbSe₃, and FeSe (Figure 3). Further, Kohn anomalies in NiTi and Ni₂MnGa point toward CDW physics existing in those materials (Figure 4). It is therefore the aim of this next subsection to discuss exemplary shape memory alloys in view of their electronic driving forces.

4.2.1. NiTi-Based Shape Memory Alloy

Today, NiTi is commercially the most successful shape memory alloy,^[106] known by its brand name Nitinol.^[107] It is used in medical applications as stents or orthodontic wires, in braces, as actuators in valves, switching, or coupling devices.^[108–112] A good level of understanding has been reached on functional properties,^[113,114] effects of compositions and microstructures,^[115,116] processing,^[117–119] functional and structural fatigue,^[120–122] and corrosion behavior.^[123] Though named shape memory alloy, NiTi is not an alloy as high and low temperature phases are ordered. The high temperature phase is of B2 type, while the low temperature phase has a B19' structure.^[124] Additions of ternary elements such as Cu, Pd, Fe destabilize the B19' martensite and promote the formation of orthorhombic B19 or R phase.^[124] Point defects, internal interfaces, and precipitates significantly affect the phase transformation

behavior.^[115,125,126] Current research trends aim for a better understanding of microstructural aspects,^[127] the development and application of high temperature^[128,129] and high entropy shape memory alloys,^[130,131] low fatigue,^[121,122] caloric effects,^[130,132–134] and additive manufacturing.^[135,136]

The importance of electronic aspects of martensitic transformations in NiTi-based shape memory alloys has often been pointed out in the literature. Shabalovskaya et al.^[137,138] conducted early research on electronic aspects and proposed the formation of a CDW.^[138] Zhao et al.^[139] discussed nesting of the Fermi surface in [110] direction. Hatcher et al.^[140] have concluded from atomistic simulations that a CDW may form which displays a structural instability of the B2 phase. The authors suggest a barrier-less mechanism for the martensitic transformation path in NiTi which is enabled by low resistance to shear (small C_{44} and C' elastic constants) and instabilities in the electronic structure and phonon spectrum of the B2 structure. They suggest a direct connection between the structural evolution between B2 and B19' and the simultaneous changes in the electronic structure. The transformation between the high- and the low-temperature phase is driven by anomalies in the Fermi surface and the phonon spectrum.^[140] Zarinejad and Liu^[141,142] studied the role of valence electrons with respect to phase transformation temperatures in a large number of NiTi-based shape memory alloys (e.g., NiTi, NiTiHf, NiTiZr, etc.). They found that generally for valence electron numbers between 5 and 7.5, the martensite start temperature almost linearly decreases with increasing valence electron concentration. The latter represents a parameter depending on valence electron count and atomic size. However, the compiled data show a significant scatter, and thus, the valence electron concentration hypothesis only captures the overall trend roughly. Employing Hall measurements, it was recently shown that the anomaly of the resistivity in NiTi is caused by a strong reduction of the charge carrier concentration at the phase transition (see Figure 3), adding an additional argument to the interpretation that a CDW phase forms at the displacive phase transition in NiTi.^[28]

4.2.2. Ti-Ta-Based Shape Memory Alloy

In addition to NiTi, also Ti-Ta-based alloys show the shape memory effect. They have a β -Ti structure, substitutionally alloyed with ≈ 12 –35 at% Ta. It is interesting to contrast the findings of the NiTi-based shape memory alloys with Ti-Ta-based ones. Different from the highly ordered NiTi compounds, Ti-Ta alloys are disordered. Transition metals favor the bcc structure for half full band as the bcc density of states is more bimodal than the density of states of the fcc or hcp structures and therefore allows for a lower band energy, while at nearly full or empty bands the skewed density of states of the more close-packed phases is stabilized. An example of this crossover can be found in Ti-Ta-based alloys, which form a close-packed phase at low d-electron count for Ti to bcc at half-full d-band for Ta. At the tipping point between close-packed and bcc stability there is room for competing phases that enable displacive phase transitions. In Ti-Ta-based alloys, the energy difference between the austenite phase and the martensite phase changes smoothly with composition.^[143] The composition dependence of the energy difference between the phases can

be rationalized simply from d-valence count, that is, the structural energy difference between austenite and martensite is determined by band filling.^[143] By further taking into account differences in phonon entropies between austenite and martensite, the change of phase transition temperature with composition can be predicted.^[144] Ti-Ta cannot be used directly as a shape memory alloy, because precipitation of an interfering phase (ω -phase) contributes to a rapid degradation of the shape memory effect. By alloying suitable elements, this precipitation phase can be destabilized with respect to austenite and martensite,^[145] enabling application.

4.2.3. Ni₂MnGa-Based Magnetic Shape Memory Alloy

The magnetic shape memory alloy Ni₂MnGa is an example of the competition between the electronic, phononic, and magnetic ordering. Amongst those materials which present coupled displacive-magnetic phase transitions, in particular the NiMn-based Heusler compounds arouse considerable attention.^[146,147] They promise potential applications such as magnetocaloric cooling and actuation based on the magnetic shape memory effect.^[146,147]

Since their discovery, numerous Ni₂Mn_{1+x}Z_{1-x} (Z = Al, In, Sb, Sn, Ga) Heusler compounds have been found to exhibit the magnetic shape memory effect.^[17,148–150] The phase transition in all these compounds is related to an interplay between different order parameters with their own symmetry properties, namely the magnetic order parameter and the elastic softening and stiffening. Additional to the magnetic driving forces, in Ni₂MnGa, electronic instabilities play an important role, leading to modulated and intermediate phases, with martensitic transformation started but not yet completed. Each of these order parameters couples not only with the strain, but also directly with each other or indirectly via the jointly resulting strain. Fundamental questions arise, which will be discussed below.

- 1) Which phase transitions are the most crucial for phonon softening or the other way round—How crucial is the phonon softening for the phase transition?
The phase transition austenite \rightarrow martensite
The phase transition austenite \rightarrow modulated martensite
The phase transition austenite \rightarrow intermediate martensite
The phase transition intermediate martensite \rightarrow modulated martensite.
- 2) How do the influence of magnetic order and external magnetic field act as stimuli for the phase transition?
- 3) Considering (1) and (2), are nesting vectors of the Fermi surface identifiable that are also consistent with phonon softening?
- 4) Is there a pseudo-gap in the Fermi energy under the influence of magnetic order and external magnetic field as stimuli?

For the stoichiometric Heusler compound Ni₂MnGa, the answers to these questions are accessible in the literature^[31,151–158] and are summarized in Figure 5 as a function of the underlying transformations. This summary is possible through a

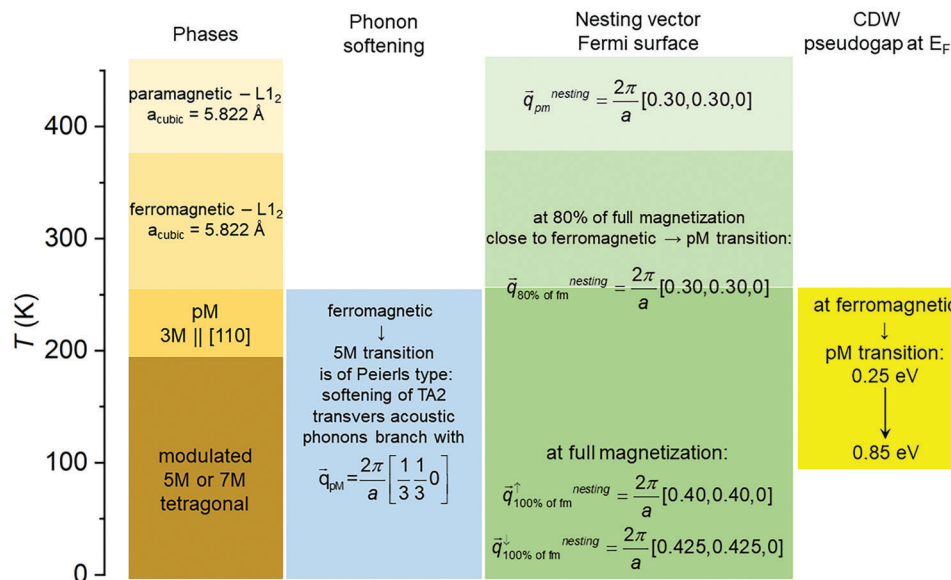


Figure 5. Ni_2MnGa as a prototype material for competing magnetic, electronic, and structural degrees of freedom at the displacive phase transition. CDW characteristics of the $L2_1$ -ordered magnetic shape memory Heusler compound Ni_2MnGa . Phase relations,^[151,152] phonon softening,^[31,153–155] nesting vectors in Fermi surface,^[156,157] and CDW pseudo gap^[158] as a function of the corresponding phase range in units of temperature. Subscripts refer to the magnetic state (pm: paramagnetic, fm: 100% ordered ferromagnetic state, 80% ordering of the magnetization during the paramagnetic to ferromagnetic phase transition). Note that the nesting vector in the ferromagnetic state differs between the majority up-arrow and the minority down-arrow spin channel.

combination of sophisticated ab initio theoretical work as well as experimental methods such as high-resolution transmission electron microscopy (HRTEM), inelastic neutron scattering (INS), positron annihilation, and photoemission studies over more than a decade of research. In addition, high quality Ni_2MnGa single crystals have been prepared and investigated for most of the experimental work. The phase transformation sequence shows the complicated microstructural relationships of the displacive phase transition in Ni_2MnGa . This happens entirely in the region of ferromagnetic ordering and contains a pre-martensitic (pM) intermediate phase, which the CDW already initiates. Thus, the pM \rightarrow M5 transformation can be attributed to the EPC type although the associated TA_2 transverse acoustic phonon branch does not show complete softening, but is at least very low. Most interesting is that the nesting effect is exactly the same as that of the observed phonon softening. This strongly suggests that the nesting of the Fermi surface could be the driving force for phonon softening in the ferromagnetic phase down to the temperature at which the pre-martensitic transition occurs.

Finally, photoemission measurements indicate that the pseudo-gap also occurs at the onset of the pre-martensite phase at 270 K. Simultaneous with the pseudo-gap, spectral weight transfer is observed over a much larger energy range of 0.25 to 0.85 eV binding energy.^[158] The associated CDW state persists in the martensite phase down to 100 K.

In summary, the investigation of electronic instabilities at the displacive phase transition opens an exciting area of research that awaits transfer to other magnetic shape memory Heusler compounds. Whether these results are transferable to other magnetic shape memory Heusler compounds that do not exhibit an intermediate martensite phase must be left to future research efforts.

4.3. Superconductors

Conventional superconductivity, where superconductivity arises from e–ph interaction, and displacive phase transitions are connected, even though they do not necessarily occur at the same time. For example, displacive phase transitions of the CDW type occur in many—especially low-dimensional—superconducting material families, and it is believed that the e–ph interaction drives both CDW and a superconducting transition. It is intriguing that displacive phase transitions also occur frequently in unconventional superconductors in close proximity to the superconducting phase in their (e.g., temperature-composition) phase diagrams. Importantly, displacive phase transitions in superconductors are naturally extremely well studied in terms of their electronic driving forces, since electronic properties are the defining features of these classes of materials. It is therefore extremely illuminating for this perspective to include the findings from this community. In particular, the experimental methodology developed in this context is pioneering in many respects.

4.3.1. Conventional Superconductors

Displacive phase transitions are known to occur in many famous superconductors above the phase transition into the superconducting state. A striking example is the A15 “high-temperature” (at the time of their discovery) superconductors, such as Nb_3Sn ^[159] and V_3Si ,^[160] the former utilized for high-field magnets. They exhibit cubic-to-tetragonal phase transitions in close vicinity to the superconducting ones.^[161,162] Interestingly, in some V_3Si samples only the superconducting transition occurs without a displacive phase transition. This is because supercon-

ductivity gaps the EPC which is needed for the displacive phase transition. Therefore, the displacive phase transition cannot happen below the superconducting transition – only the other way around. The simultaneous occurrence of soft modes, structural instabilities, unusual temperature dependencies and superconductivity is common to all materials of this A15 class and has excited a debate about the role of displacive phase transformations for the evolution of superconductivity early on.^[163]

More recently, several CDW materials came into focus, which show superconductivity in a region of the phase diagram where the CDW is suppressed by external parameters such as physical pressure or chemical substitution, or intercalation. A prominent example is TiSe_2 . Here, the soft phonon mode of the CDW likely plays an important role in the formation of superconductivity. Namely, the suppression of CDW order should liberate/activate the soft mode's EPC for the formation of Cooper pairs and thus support a superconducting ground state. Indeed, ab-initio calculations support such a scenario in the presence of significant EPC.^[164,165] Experimentally, the situation is less clear^[166,167] since not all EPC is contained in the soft mode^[168] and mechanisms other than EPC can also play a role.^[169] These conventional superconductors represent exciting examples, where structural instabilities are likely favorable for superconductivity because of the EPC mechanism. Recently, a displacive phase transition was also reported in the elemental superconductor Nb,^[170] but featured extremely small structural distortions and therewith difficult to be detected by standard methods of structure research, and also not understood theoretically.

4.3.2. Unconventional Superconductors

Displacive phase transitions were also reported in a number of unconventional superconductors, for which superconductivity is mediated by a mechanism other than (pure) EPC. Some of the famous high-temperature superconducting perovskite copper oxides, such as $\text{YBa}_2\text{Cu}_3\text{O}_{6+\delta}$ (YBCO) and $\text{La}_{2-x}\text{Ba}_x\text{CuO}_4$ (LBCO), feature a prominent tetragonal-to-orthorhombic phase transition.^[171–173] In LBCO, the structural distortion of the CuO_2 layers enables pinning of charge stripe order whose appearance coincides with the structural transition and correlates with a significant drop of the superconducting T_c at $x = 1/8$.^[174,175] Charge order in cuprates was first discovered in the form of such stripe order, more specifically as a nanoscale array of unidirectional collinear spin and charge modulations.^[176] However, the static striped phase appears to occur only in La-based cuprates, while they were found to be more of a dynamic phenomenon in many other cuprates.

A much more generic and potentially universal charge-ordering phenomenon in superconducting cuprates are CDWs. CDWs have now been observed in all chemically distinct cuprate families including essentially all hole-doped cuprates as well as Nd-based electron-doped cuprates using bulk-sensitive momentum-space techniques, such as neutron and X-ray diffraction and resonant X-ray diffraction, as well as the surface-sensitive real-space technique of scanning tunneling microscopy (STM), see, for example, the reviews^[177,178] for a summary of results. In the temperature-doping phase diagram of hole-doped cuprates, a CDW dome within the pseudogap regime at moder-

ate doping levels centered at the “magical” doping of $1/8$ is now considered to be a universal feature. In addition, CDWs were found inside the superconducting dome upon suppression of superconductivity by, for example, high magnetic fields,^[179] and in the Fermi liquid state in the overdoped region.^[180] Despite their universal appearance in the phase diagram, the phenomenology of CDWs is quite broad and material-specific, with distinct CDW transition temperatures (up to about 250 K), wavevectors (in the plane typically corresponding to a charge modulation with a period of about 3–4 lattice constants along the Cu-O bond direction), dimensionalities (2D and 3D), and correlation lengths (up to about 100 lattice constants in plane and up to about 10 lattice constants out of plane).^[178] The dominant nature of CDW order in unperturbed hole-doped cuprates is 2D and short-range. This may be explained by a weak coupling of the CuO_2 planes and the effects of disorder or fluctuations, which tend to be more destructive in 2D compared with 3D.^[181] CDWs in cuprates are therefore mostly weak. The lattice distortions are typically of small amplitude, on the order of 10^{-3} lattice units, and CDW energy gap opening or Fermi surface folding in angle-resolved photoemission spectroscopy (ARPES), as known from conventional CDW materials, is not observed. A complete reconstruction of the Fermi surface occurs only when long-range CDW order sets in at high magnetic fields,^[179] which are incompatible with the ARPES technique. On the other hand, CDWs are thermodynamically robust because CDW correlations persist over a wide range of temperatures and doping in the phase diagram and compete with the superconducting state; strong CDW correlations are accompanied by suppression of the superconducting T_c , while CDW correlations are weakened at the emergence of the superconducting state upon cooling.^[175]

The CDW mechanism, particularly the link between the CDW and the electronic structure at the Fermi level, has remained largely elusive. Both Fermi surface nesting and momentum-dependent EPC have been ruled out as driving forces.^[182,183] Nevertheless, it was found that the doping dependence of the CDW wavevector is consistent with a “nesting” of the tips of the so-called Fermi arcs in underdoped $\text{Bi}_2\text{Sr}_{2-x}\text{La}_x\text{CuO}_{6+\delta}$ ($\text{Bi}2201$),^[182] and in underdoped YBCO a strong, sharp, but only partial softening of low-energy acoustic and optical phonons at the CDW wavevector was observed,^[184] consistent with the short-range nature of the CDW correlations. The CDW in cuprates was therefore classified as unconventional and its origin was generally attributed to electron correlations or many-body interactions.^[68,183] This uncertainty about the driving force behind charge order leads to the controversial question of whether the CDW is crucial for the anomalous properties of the superconducting cuprates or if it is just the by-product of a peculiar metallic state. In attempts to answer this question and uncover the CDW mechanism, the CDW in cuprates will certainly continue to provide fertile ground for elucidating the interplay of Mott physics, CDWs, and superconductivity.

4.3.3. Nematicity in Iron-Based Superconductors

The class of iron-based superconductors, with its relevant parent compounds including FeSe , BaFe_2As_2 , and LaFeAsO , has been studied intensely since 2008.^[185–187] The parent compounds

become superconducting with a maximum T_c typically of the order of 25–40 K via substitution of various elements. Apart from superconductivity, a central theme of research for these materials is nematicity, the electronically driven displacive tetragonal-to-orthorhombic structural phase transition.^[71] In most materials,—but not in the highly studied model system FeSe^[188]—antiferromagnetic order also plays a central role.

Nematicity is experimentally probed via the electronic anisotropy between the two orthorhombic axes. In particular, the direct current (dc)-resistivity anisotropy in the nematic phase is, likely, the most studied signature of nematicity in iron-based superconductors.^[189,190] Other well-studied examples of nematic electronic anisotropy are found in optical reflectivity,^[191] local magnetic susceptibility,^[192] thermoelectric properties,^[193] the electronic energy-momentum dispersion as seen by ARPES,^[194,195] or the electronic structure around defects seen in scanning tunneling microscopy (STM).^[196] Nevertheless, the mechanism of the nematic phase transition and the microscopic nature of the nematic order parameter is, however, difficult to pin down. A Pomeranchuk instability of the Fermi surface, various types of orbital order, and frustrated magnetic interactions have all been discussed as its possible driving force. The prevalent theory evokes the close-by antiferromagnetism and describes nematicity via the scenario of frustrated magnetic fluctuations.^[197] However, the case of FeSe for which the nematic phase transition occurs far from magnetic order is a challenge to this picture.^[188]

The existence of an electronic nematic order parameter, irrespective of its microscopic origin, means that there is a related susceptibility, whose measurement is a challenging task. The soft mode of the tetragonal-to-orthorhombic structural phase transition is naturally an elastic shear modulus. Indeed, softening of this shear modulus on approaching the nematic transition from the high-temperature phase is readily observed.^[198,199] Just as a finite nematic order parameter means a finite orthorhombic distortion, the softening of the elastic shear mode reflects a divergence of the nematic susceptibility. Over the last decade, multiple experimental approaches to the nematic susceptibility have been developed.^[200] A pioneering and innovative experiment provided a strong argument for an electronic origin of the structural distortion via a measurement of the electronic nematic susceptibility.^[189] Namely, samples were submitted to an external anisotropic strain. In this case, the induced resistivity anisotropy becomes a measure of the nematic susceptibility, but for a “passive” crystal lattice. Since a divergence was still observed, an electronic driving mechanism for the nematic phase transition could be concluded.

“Nematic” phase transitions have by now been reported in an increasing number of superconducting and non-superconducting quantum materials (e.g., refs. [201–206]). However, iron-based superconductors are the most prominent materials to study this displacive phase transition as their signatures are pronounced, they can be investigated with a wide range of experimental techniques, they are easily tunable via chemical substitutions and pressure, and high-quality single-crystal samples are widely available. The relation of nematicity and superconductivity is still a matter of research and nematic fluctuations appear to be favorable for superconductivity.^[207,208]

4.4. Ferroelectrics

The interplay between a displacive phase transition and other order parameters is not restricted to metals. Similar phenomena are observed at insulator-to-insulator transitions in the family of ABO_3 perovskites, for example, in the prototypical materials $BaTiO_3$, $PbTiO_3$, $SrTiO_3$, and $PbZrO_3$. Analogous to the austenitic phase in metallic shape memory materials, the parent high-temperature phase of these compounds has a high symmetry (cubic, centrosymmetric, paraelectric), low-energy phonon modes soften under cooling, and at least one displacive phase transition to a distorted phase with lower symmetry occurs under cooling. Here instabilities at high-symmetric points of the Brillouin zone play the most important role. For the prototypical ferroelectric $BaTiO_3$ three degenerate optical modes (F_{1u}) at the Γ -point soften. The eigenvector of these modes corresponds to the shift of Ti ions with a formal charge of 4+ against the O^{2-} -cage, that is, to the formation of a local dipole moment in each unit cell. Larger polarization is possible in $PbTiO_3$ as also the Pb^{2+} ions shift.^[38] At the phase transition to the ferroelectric phase, cooperative long-range ordering of dipoles sets in and the dielectric response shows a pronounced peak. Although softening of F_{1u} modes and the typical Curie–Weiss behavior expected above a ferroelectric phase transition is also observed for $SrTiO_3$, quantum fluctuations suppress the phase transition down to zero temperature (quantum paraelectric phase).^[209,210]

In another subclass of materials, represented by the prototypical material $PbZrO_3$, a peak in the dielectric response has been reported between phases without spontaneous polarization and has been related to the onset of antiferroelectric ordering. In both the antiferroelectric and quantum paraelectric materials, soft modes at the zone boundary may characterize the structure of the low temperature phases related to different rotation and distortion of the O octahedra.^[211,212] The antiferroelectric phase of $PbZrO_3$ is still under active debate and it has been reported that the transition may be the consequence of the coupled freezing of several zone boundary modes and modes at incommensurable points.^[38,213,214] In close analogy to shape memory alloys, there is an ongoing discussion on intermediate phases at the transition related to the complex interplay of phonon modes and the microstructure.^[214]

Although ferroelectric transitions have been characterized as displacive phase transition related to phonon softening early,^[215,216] this interpretation cannot explain all features of the phase transition. Already in the 60th of the last century, a competing interpretation assumed an order-disorder transition of the local dipoles between the $8 \langle 111 \rangle$ directions,^[217–219] and the transitions are often discussed as being of mixed displacive order-disorder type.^[36,220]

All these transitions in the prototypical materials are coupled structural ferroic transitions. As reviewed in ref. [221] even in wide band gap insulators the electronic degrees of freedom cannot be decoupled from the structural-ferroic transition and all distortions of the cubic lattice are controlled by changes in the electronic structure.^[222] In particular, O^{2-} ions that are not stable on their own and whose bonding character depends strongly on the atomic environment (coordination, distances, etc.) play an important role in ferroelectric transitions. The electronic driving force for the ferroelectric instability is the pseudo-Jahn Teller effect;

even without degenerate orbitals, the system may lower its energy by the splitting of hybrid orbitals which lifts inversion symmetry as needed for ferroelectric polarization. As shown by Cohen^[223] a ferroelectric displacement of the ions reduces the long-range electrostatic energy but induces an energy penalty as some ions come closer to each other. The latter can be compensated if the ions change their hybridization during the displacement. Particularly for Ti-O₆, the lowest unoccupied orbitals are the Ti-d orbitals which can re-hybridize easily. For Pb and Bi ions on the A-side, furthermore their electronic 6s²6p⁰ lone pair configuration is unstable against mixing with a low-lying excited 6s¹6p¹ state and may result in broken inversion symmetry by the pseudo-Jahn Teller effect.^[224] Analogously, also octahedra rotations are related to the pseudo-Jahn Teller effect. Typically, the underlying shift of charges is monitored by the Born effective charge tensor whose elements for Ti in an O-environment are larger than 7 and reach about 6 for Pb.^[225]

Due to the broken symmetry in the ferroelectric phases, the different B-O distances result in alternating charges along the ferroelectric axis.^[226]

5. Perspective for Research

What is the added value of an interdisciplinary approach to displacive phase transitions?

An important area in which a scientific gap in knowledge can be identified is the possible connection between CDW physics and the shape memory effect. This starts with the question if the electronic ordering and the pseudo-gap of a CDW can actually be proven in the NiTi and Ni₂MnGa-based shape memory alloys. If so, how does the CDW form with respect to compositional changes? To date, the understanding of the (potential) electronic origin of this displacive phase transition has not yet been systematically utilized for the design and optimization of the material. For example, if in NiTi and in Ni₂MnGa the martensitic phase transformations were related to CDW phenomena, rules for how substitutional elements stabilize the different phases should be derived based on the electronic contribution to the driving forces. Questions might be: How does substitution modify the Fermi surface, in particular the nesting, and thereby the characteristics of the phase transition? In the case of NiTi, how does this promote the formation of the R-phase, stabilize the B19' phase, or favor the transition to a strain glass phase? In the case of Ni₂MnGa, do the electronic driving forces depend on the electron spin? Adding more complexity, how do microstructural defects which could be introduced through materials' processing or functional or mechanical fatigue affect the formation of the CDW? Is there a direct link between fatigue mechanisms and the electronic driving forces of the phase transition? Is aging connected to this electronic effect, for example, in the sense that the destabilization of the CDW corresponds to a destabilization of the martensitic phase?

In particular, the generalization of these questions contains fundamental physics: Does CDW physics play a role in shape memory alloys in more general or even in the shape memory effect as such? Here, especially the comparison of NiTi with another shape memory alloy, Ti-Ta, might be insightful, since Ti-Ta shows the shape memory effect but in a disordered alloy rather than in an ordered compound.

Quite similar to the questions that have arisen around the combination of CDW and shape memory alloys, important open questions about the combination of CDW and high temperature superconductivity are: What is the origin of CDW, that is, the microscopic mechanism? Is the mechanism universal or material specific? What is the role of electronic correlations? What is the role of the crystal lattice or periodic lattice distortion of CDW? How are CDW and superconductivity intertwined? What does this look like in real space: homogeneous coexisting orders, domains separated at the nanoscale, or superconductivity-induced topological defects in CDW domains? What is the interplay between CDW and the other phases (pseudogap, strange metal) in the phase diagram? What is the connection between CDW and Fermi arcs (pseudogap phase)? How are CDW and deviations from T-linear resistance related (strange metal phase)? What is the relationship between CDW and SDW in La-based cuprates? With this perspective, we add another aspect to this complex topic: What is the role of the displacive phase transition that often occurs at much higher temperature (e.g., in YBCO during the synthesis or annealing), in relation to the forming CDW? In other materials, the formation of CDW is closely linked to this displacive phase transition – how does this behave in high-temperature superconductors?

The studies on pnictide superconductors showing displacive phase transitions lead us to ask more generally to what extent displacive phase transitions are electronically driven. In the case of the nematic phase transition of iron-based superconductors, it was proven with carefully developed experimental techniques that the displacive phase transition is electronically driven. Electronic motifs also seem to play an important role in at least some shape memory alloys. In this perspective, the common motifs of CDW, Mott transitions, or electronic nematic phase were revealed. Does this mean that electronic driving forces are highly relevant for displacive phase transitions in general or is the case of the nematic phase transition of iron-based superconductors an outlier within a class of phase transitions that otherwise has structural causes?

How can we proceed to find scientifically sound answers to these questions? An important possibility here lies in the interdisciplinary approach that has advantages, especially in the field of experimental and computational methods. New developments in the field of experimental art or computational methods often take place within a specific community. By applying these new developments to similar problems in neighboring research areas, the significance and impact inevitably increase. The following compilation cannot be complete, but it shows a path that research could take in the future.

Ferroelectrics are extensively studied by X-ray methods (especially diffraction) and spectroscopic techniques (especially optical). In comparison, this is true for shape memory alloys and also caloric materials to a much lesser extent. In particular, spectroscopic techniques that generally target electron behavior seem to have been little used for these two classes of materials.

In photoelectron spectroscopy (PES), there have been two important new developments in the last decade—to nanometer spatial resolution and to femtosecond time resolution using sharply focused or ultrashort pulsed XUV/X-ray radiation. Nanometer PES provides a view of the local electronic structure, while femtosecond PES can be used to track ultrafast electronic dynamics

in real time. Thus, electronic microstructures on one hand and fundamental electronic interactions on the other hand can be directly spectroscopied, and spatial and temporal couplings between electronic and lattice degrees of freedom can be elucidated. This is particularly relevant for the microscopic understanding of displacive phase transitions and has been demonstrated highly successfully on CDW materials. However, for classes of materials such as shape memory alloys and caloric materials, such advanced PES experiments have rarely (if ever) been performed, most likely because of insufficient sample or surface quality or because the potentially significant role of electrons has partly been ignored in these materials. In particular, the necessary high quality of the surfaces is certainly a considerable challenge for materials that do not have suitable cleavage planes, cannot be delaminated, oxidize immediately at the surface, as well as form deformation zones under small mechanical loads. On the other hand, the gain in knowledge would be considerable if surface preparation could be brought under control.

INS is the classic momentum-resolved technique to investigate lattice dynamical properties of solids with ground-breaking work for the understanding of novel ground states such as superconductivity,^[227–230] CDW-order,^[231,232] and ferroelectric-driven lattice distortions.^[233,234] However, state-of-the-art neutron time-of-flight and inelastic X-ray spectrometers allow much more comprehensive and detailed investigations. Therefore, several long known ferroelectric^[235,236] and CDW materials^[29] have been re-investigated in part with new parameters such as high-pressure.^[168] These studies show the impact of anharmonic lattice vibrations on the materials' properties and basic mechanisms such as phonon-momentum dependent EPC that drives electronic phase transitions. We believe that interesting materials such as shape memory alloys or caloric materials are underrepresented in current INS and inelastic X-ray scattering research though their peculiar lattice dynamical properties are far from understood. Thus, there is a high potential for new discoveries and improved material understanding for applications in the investigation of lattice dynamics using state-of-the-art neutron and X-ray spectroscopy.

In the electronically correlated matter community, displacive phase transitions have been characterized in terms of their elasto-resistance response using an extremely sophisticated methodology. This characterization has existed for semiconductors for quite some time, but has been pursued more and more intensively in recent years, especially with respect to various symmetries, linear versus nonlinear elasto-resistance response, etc. There are now various techniques that can be used under in situ tuneable uniaxial pressure, from elasto-resistivity, to elasto-X-ray diffraction, elasto-STM, and even elasto-ARPES. For example, the combination of elasto-resistance with elastic-modulus measurements and elasto-X-ray diffraction seems especially promising. Note that the achievable strains are often still small ($\lesssim 1\%$ and sometimes much less). As a consequence of these considerable methodological advances, it could be concluded for the nematic phase transition of iron-based superconductors, that it is of electronic origin. Similar conclusions have so far been precluded for other classes of materials. In addition, the development of various “detwinning” techniques in the same community allows to measure a variety of properties, up to neutron scattering, ARPES, magnetic susceptibility, etc. on monodomain crystals.

Related to the question of electronic driving forces in general is the question of the role of conduction electrons. It occurs that characterization of the charge carrier density and mobility (e.g., Hall measurements, THz spectroscopy) has not been systematically performed on all relevant metals undergoing displacive phase transitions. Related, how do screening effects influence this phase transition? Is it possible to analyze the electronic transport characteristics spin-resolved, for example, in magnetic metals?

Transmission electron microscopy has been extensively applied to shape memory alloys and ferroelectric materials. Similar thorough microscopic studies are not equally common in the correlated materials community, for example. The development of in situ methods allows increasingly precise measurement of microstructure, electronic, and vibronic properties, and their responses to external stimuli at all length scales. Especially electronic and magnetic polarization can be visualized with nanometer spatial resolution by advanced microscopy techniques. The combination of HRTEM capabilities with various detectors allows to extract information about the atomic structure, chemical nature, magnetic and electrical properties, and their interactions from one sample, including temperature-dependent studies by in situ heating or cooling. For phase transformations, the visualization and measurement of electric and magnetic fields at the atomic level is fundamental, since they directly determine the magnetic and electronic properties of the phases. In any HRTEM equipped with an electron energy-loss spectroscopy (EELS) detector,^[237] the electron energy-loss magnetic chiral dichroism^[238,239] effect can be characterized to determine the magnetic properties of atoms, that is, the spin and the corresponding magnetic orbital moment. Differential phase contrast (DPC) imaging^[240] to determine the electronic properties, is based on the shift of the center of gravity of the illumination intensity in the detector plane, which can be precisely measured with a modern segmented DPC detector to determine the local charge density of these phases. The combination of HRTEM and DPC similarly offers fantastic opportunities for measuring magnetic properties. Not only can the intrinsic magnetic properties of the phases be measured, but also their interactions.^[241]

When it comes to understanding the microstructure, so far mostly strain aspects were taken into consideration. At least for insulating materials, also discontinuities in the polarization or charges at interfaces play prominent role. However, the role of discontinuities of other order parameters (e.g., spin) at the phase boundary is often neglected.

Many developments in computational methods also took place in the community of electronically correlated matter. However, the computational effort is usually limited here. Some of the raised questions could not be addressed comprehensively in the past simply because of much too high computational demands. However, some of them might be possible to address in the future.

It will be important to see how the electronic correlations, which cannot be captured within DFT, affect the nature of the phase transitions, including the changes in the corresponding susceptibilities. Here a combination of dynamical mean-field theory (DMFT) on top of the DFT band structure and the effective modeling based on the tight-binding projections into Wannier orbitals and construction of the effective field theory is necessary.

The role of EPC and the general equal footing treatment of electronic and phononic degrees of freedom can currently be addressed at the model Hamiltonian level, but hardly for real materials, as this is still too costly. Atomic forces for low-symmetry materials are implemented in some DFT+DMFT codes, but are rarely studied in detail so far, because they are either also very costly or hard to converge. Entropy descriptions at finite temperature to a true modeling of the free energy (with correlations), are for real materials still hardly existent, but descriptions use pure energy considerations so far. Also, phononic or local-momentum spin contributions are hardly considered in the real description of phase concurrences. Dynamical fluctuations of such transformations (k - and ω -dependent coupled e -ph self-energies/susceptibilities) are not yet discussable. The description of nematic phenomena has gained a lot of importance, but for challenging materials (many orbitals, low symmetry), the computational treatment is only possible to a limited extent, and often again only at the model level. In general, lattice susceptibilities of any kind have become possible for materials in the last 10 years, but especially for multi-orbital systems, they are often very difficult to access. Low temperatures and even the (non-adiabatic) connection to the phonon system remain difficult and are hardly implemented. Also, molecular dynamics approaches for strongly-correlated systems have been proposed recently, but are still in their infancy. With ever-improving computational capabilities, both on the hardware side and on the code implementation side, addressing these questions will open up a fascinating deeper understanding of the physics of displacive phase transitions in the future.

6. Concluding Remarks

Displacive phase transitions in as diverse material classes as shape memory alloys, electronically correlated materials, superconductors, and ferroelectrics share common microstructural, electronic, and phononic signatures. The common microstructure is characterized by twinning, often in a hierarchical arrangement. Common electronic signatures manifest themselves in transport anomalies, caused by a reduction of the charge carrier density and an increase of the charge carrier mobility at the phase transition, a change of the charge order, up to a change of the nature of the charge carriers as such. Common phononic signatures are phonon softening, often combined with Fermi surface nesting and caused by EPC. The disentanglement of these coupled structural, electronic, and magnetic phenomena provides an almost inexhaustible source of beautiful science that can and will be used to develop materials with excellent functional properties. Additionally, these displacive phase transitions are important for various applications because of their functional properties. Amongst them, explicitly shape memory alloys, many superconductors, and ferroelectrics are discussed within this perspective. While these applications significantly push material developments and their understanding in the respective communities, the experimental and computational evidence compiled opens up very fundamental questions that are of transdisciplinary nature. These concern in particular the relation between mechanisms underlying the various displacive phase transitions. The question of generalization is now compelling.

Acknowledgements

Open access funding enabled and organized by Projekt DEAL.

Conflict of Interest

The authors declare no conflict of interest.

Keywords

charge density wave, ferroelectricity, martensitic phase transition, shape memory alloys, superconductivity

Received: March 10, 2023

Revised: May 25, 2023

Published online:

- [1] V. Y. Topolov, *Heterogeneous Ferroelectric Solid Solutions: Phases and Domain States*, Vol. 151, Springer, Berlin **2011**, p. 172.
- [2] A. Grünebohm, M. Marathe, R. Khachatryan, R. Schiedung, D. C. Lupascu, *J. Phys.: Condens. Matter* **2022**, *34*, 073002.
- [3] J. Erhart, W. Cao, *J. Appl. Phys.* **2003**, *94*, 3436.
- [4] G. Metrat, *Ferroelectrics* **1980**, *26*, 801.
- [5] M. S. Wechsler, D. S. Liebermann, T. A. Read, *Trans. Am. Inst. Min., Metall. Pet. Eng.* **1953**, *197*, 1503.
- [6] G. F. Nataf, E. K. H. Salje, *Ferroelectrics* **2020**, *569*, 82.
- [7] T. Waitz, in *EMC 2008 14th European Microscopy Congress 1–5 September 2008, Aachen, Germany* (Eds: S. Richter, A. Schwedt), Springer, Berlin, Heidelberg **2008**, pp. 507–508.
- [8] R. D. James, Z. Zhang, *Magnetism and Structure in Functional Materials*, vol. 79 (Eds: L. Mañosa, A. Planes, A. Saxena), Springer, New York **2005**, pp. 159–175.
- [9] R. Niemann, A. Backen, S. Kauffmann-Weiss, C. Behler, U. K. Rößler, H. Seiner, O. Heczko, K. Nielsch, L. Schultz, S. Fähler, *Acta Mater.* **2017**, *132*, 327.
- [10] S. Schwabe, R. Niemann, A. Backen, D. Wolf, C. Damm, T. Walter, H. Seiner, O. Heczko, K. Nielsch, S. Fähler, *Adv. Funct. Mater.* **2021**, *31*, 2005715.
- [11] G. Arlt, P. Sasko, *J. Appl. Phys.* **1980**, *51*, 4956.
- [12] J. S. Bowles, J. K. Mackenzie, *Acta Metall.* **1954**, *2*, 129.
- [13] A. G. Khachatryan, S. M. Shapiro, S. Semenovskaya, *Phys. Rev. B* **1991**, *43*, 10832.
- [14] Y. M. Jin, Y. U. Wang, A. G. Khachatryan, J. F. Li, D. Viehland, *Phys. Rev. Lett.* **2003**, *91*, 197601.
- [15] S. Kaufmann, R. Niemann, T. Thersleff, U. K. Rößler, O. Heczko, J. Buschbeck, B. Holzapfel, L. Schultz, S. Fähler, *New J. Phys.* **2011**, *13*, 053029.
- [16] R. Tickle, R. D. James, T. Shield, M. Wuttig, V. V. Kokorin, *IEEE Trans. Magn.* **1999**, *35*, 4301.
- [17] N. Teichert, D. Kucza, O. Yildirim, E. Yuzuak, I. Dincer, A. Behler, B. Weise, L. Helmich, A. Boehnke, S. Klimova, A. Waske, Y. Elerman, A. Hütten, *Phys. Rev. B* **2015**, *91*, 184405.
- [18] S. Matzen, O. Nesterov, G. Rispiens, J. A. Heuver, M. Biegalski, H. M. Christen, B. Noheda, *Nat. Commun.* **2014**, *5*, 4415.
- [19] C. L. Jia, K. Urban, M. Mertin, S. Hoffmann, R. Waser, *Philos. Mag. A* **1998**, *77*, 923.
- [20] N. H. Andersen, B. Lebech, H. F. Poulsen, *Phys. C* **1990**, *172*, 31.
- [21] M.-G. Blanchin, V. S. Teodorescu, J. Garcia-Lopez, J. Siejka, R. Bisaro, L. M. Mercandalli, *Philos. Mag. A* **1996**, *74*, 151.
- [22] M. A. Tanatar, A. E. Böhrer, E. I. Timmons, M. Schütt, G. Drachuck, V. Taufour, K. Kothapalli, A. Kreyssig, S. L. Bud'ko, P. C. Canfield, R. M. Fernandes, R. Prozorov, *Phys. Rev. Lett.* **2016**, *117*, 127001.

- [23] A. Srivastava, H. Rotella, S. Saha, B. Pal, G. Kalon, S. Mathew, M. Motapothula, M. Dykas, P. Yang, E. Okunishi, D. D. Sarma, T. Venkatesan, *APL Mater.* **2015**, 3, 026101.
- [24] N. P. Ong, P. Monceau, *Solid State Commun.* **1978**, 26, 487.
- [25] N. P. Ong, P. Monceau, *Phys. Rev. B* **1977**, 16, 3443.
- [26] Y. Sun, S. Pyon, T. Tamegai, R. Kobayashi, T. Watashige, S. Kasahara, Y. Matsuda, T. Shibauchi, *Phys. Rev. B* **2015**, 92, 144509.
- [27] M. D. Watson, T. Yamashita, S. Kasahara, W. Knafo, M. Nardone, J. Béard, F. Hardy, A. Mccollam, A. Narayanan, S. F. Blake, T. Wolf, A. A. Haghhighrad, C. Meingast, A. J. Schofield, H. V. Löhneysen, Y. Matsuda, A. I. Coldea, T. Shibauchi, *Phys. Rev. Lett.* **2015**, 115, 027006.
- [28] A. Kunzmann, J. Frenzel, U. Wolff, J. W. Han, L. Giebeler, D. Piorunek, M. Mittendorff, J. Scheiter, H. Reith, N. Perez, K. Nielsch, G. Eggeler, G. Schierning, *Mater. Today Phys.* **2022**, 24, 100671.
- [29] F. Weber, S. Rosenkranz, J.-P. Castellán, R. Osborn, R. Hott, R. Heid, K.-P. Bohnen, T. Egami, A. H. Said, D. Reznik, *Phys. Rev. Lett.* **2011**, 107, 107403.
- [30] H. Tietze, M. Mullner, B. Renker, *J. Phys. C: Solid State Phys.* **1984**, 17, L529.
- [31] A. Zheludev, S. M. Shapiro, P. Wochner, A. Schwartz, M. Wall, L. E. Tanner, *Phys. Rev. B* **1995**, 51, 11310.
- [32] S. Ener, J. Neuhaus, W. Petry, R. Mole, K. Hradil, M. Siewert, M. E. Gruner, P. Entel, I. Titov, M. Acet, *Phys. Rev. B* **2012**, 86, 144305.
- [33] P. W. Anderson, E. I. Blount, *Phys. Rev. Lett.* **1965**, 14, 217.
- [34] N. A. Spaldin, M. Fiebig, M. Mostovoy, *J. Phys.: Condens. Matter* **2008**, 20, 434203.
- [35] Y. Song, X. Chen, V. Dabade, T. W. Shield, R. D. James, *Nature* **2013**, 502, 85.
- [36] K. A. Müller, Y. Luspín, J. L. Servoin, F. Gervais, *J. Phys. Lett.* **1982**, 43, 537.
- [37] B. Himmetoglu, A. Janotti, H. Peelaers, A. Alkauskas, C. G. Van De Walle, *Phys. Rev. B* **2014**, 90, 241204.
- [38] Ph. Ghosez, E. Cockayne, U. V. Waghmare, K. M. Rabe, *Phys. Rev. B* **1999**, 60, 836.
- [39] A. Grünebohm, M. Siewert, C. Ederer, P. Entel, *Ferroelectrics* **2012**, 429, 31.
- [40] U. Aschauer, N. A. Spaldin, *J. Phys.: Condens. Matter* **2014**, 26, 122203.
- [41] K. F. Garrity, *Phys. Rev. B* **2018**, 97, 024115.
- [42] S. Premkumar, S. Radhakrishnan, V. L. Mathe, *J. Mater. Chem. C* **2021**, 9, 4248.
- [43] S. Kim, K. Kim, C.-J. Kang, B. I. Min, *Phys. Rev. B* **2013**, 87, 195106.
- [44] M. A. Uijtewaald, T. Hickel, J. Neugebauer, M. E. Gruner, P. Entel, *Phys. Rev. Lett.* **2009**, 102, 035702.
- [45] T. Hickel, M. Uijtewaald, B. Grabowski, J. Neugebauer, *J. Phys.: Condens. Matter* **2008**, 20, 064219.
- [46] T. Büsgen, J. Feydt, R. Hassdorf, S. Thienhaus, M. Moske, M. Boese, A. Zayak, P. Entel, *Phys. Rev. B* **2004**, 70, 014111.
- [47] S. Ehsan, M. Arrigoni, G. K. H. Madsen, P. Blaha, A. Tröster, *Phys. Rev. B* **2021**, 103, 094108.
- [48] J. M. Skelton, L. A. Burton, S. C. Parker, A. Walsh, C.-E. Kim, A. Soon, J. Buckeridge, A. A. Sokol, C. R. A. Catlow, A. Togo, I. Tanaka, *Phys. Rev. Lett.* **2016**, 117, 075502.
- [49] O. Hellman, P. Steneteg, I. A. Abrikosov, S. I. Simak, *Phys. Rev. B* **2013**, 87, 104111.
- [50] G. D. Samolyuk, Y. N. Osetsky, G. M. Stocks, J. R. Morris, *Phys. Rev. Lett.* **2021**, 126, 025501.
- [51] W. I. Choi, D. J. Yang, D. W. Jung, W.-J. Son, M. Shim, I. Jang, D. S. Kim, *MRS Commun.* **2021**, 11, 436.
- [52] N. R. Werthamer, *Phys. Rev. B* **1970**, 1, 572.
- [53] T. Tadano, S. Tsuneyuki, *Phys. Rev. B* **2015**, 92, 054301.
- [54] L. Monacelli, R. Bianco, M. Cherubini, M. Calandra, I. Errea, F. Francesco, *J. Phys.: Condens. Matter* **2021**, 33, 363001.
- [55] J. B. Haskins, H. Malmir, S. J. Honrao, L. A. Sandoval, J. W. Lawson, *Acta Mater.* **2021**, 212, 116872.
- [56] J. Tidholm, O. Hellman, N. Shulumba, S. I. Simak, F. Tasnádi, I. A. Abrikosov, *Phys. Rev. B* **2020**, 101, 115119.
- [57] S. Kadhodaei, A. Van De Walle, *Comput. Phys. Commun.* **2020**, 246, 106712.
- [58] T. A. Mellan, H. Wang, U. Schwingenschlögl, R. Grau-Crespo, *Phys. Rev. B* **2019**, 99, 064113.
- [59] E. J. W. Verwey, *Nature* **1939**, 144, 327.
- [60] E. J. W. Verwey, P. W. Haayman, *Physica* **1941**, 8, 979.
- [61] N. F. Mott, R. Peierls, *Proc. Phys. Soc.* **1937**, 49, 72.
- [62] R. E. Peierls, *Quantum Theory of Solids*, Clarendon Press, Oxford **1955**.
- [63] S. B. Roy, *Mott Insulators: Physics and Applications*, 6th ed., IOP Publishing, Bristol **2019**.
- [64] B. Renker, H. Rietschel, L. Pintschovius, W. Gläser, P. Brüesch, D. Kuse, M. J. Rice, *Phys. Rev. Lett.* **1973**, 30, 1144.
- [65] M. Hoesch, A. Bosak, D. Chernyshov, H. Berger, M. Krisch, *Phys. Rev. Lett.* **2009**, 102, 086402.
- [66] M. Hoesch, X. Cui, K. Shimada, C. Battaglia, S.-I. Fujimori, H. Berger, *Phys. Rev. B* **2009**, 80, 075423.
- [67] M. D. Johannes, I. I. Mazin, *Phys. Rev. B* **2008**, 77, 165135.
- [68] X. Zhu, J. Guo, J. Zhang, E. W. Plummer, *Adv. Phys. X* **2017**, 2, 622.
- [69] V. Polinger, P. Garcia-Fernandez, I. B. Bersuker, *Phys. B* **2015**, 457, 296.
- [70] I. B. Bersuker, *Appl. Phys. Lett.* **2015**, 106, 022903.
- [71] A. E. Böhmer, J.-H. Chu, S. Lederer, M. Yi, *Nat. Phys.* **2022**, 18, 1412.
- [72] A. W. Overhauser, *Phys. Rev. Lett.* **1984**, 53, 64.
- [73] G. Ernst, C. Artner, O. Blaschko, G. Krexner, *Phys. Rev. B* **1986**, 33, 6465.
- [74] H. G. Smith, *Phys. Rev. Lett.* **1987**, 58, 1228.
- [75] H. G. Smith, R. Berliner, J. D. Jorgensen, M. Nielsen, J. Trivisonno, *Phys. Rev. B* **1990**, 41, 1231.
- [76] G. J. Ackland, M. Dunuwille, M. Martinez-Canales, I. Loa, R. Zhang, S. Sinogeikin, W. Cai, S. Deemyad, *Science* **2017**, 356, 1254.
- [77] M. Hutcheon, R. Needs, *Phys. Rev. B* **2019**, 99, 014111.
- [78] P. Jerabek, A. Burrows, P. Schwerdtfeger, *Chem. Commun.* **2022**, 58, 13369.
- [79] V. V. Struzhkin, M. I. Erements, W. Gan, H.-K. Mao, R. J. Hemley, *Science* **2002**, 298, 1213.
- [80] K. Shimizu, H. Ishikawa, D. Takao, T. Yagi, K. Amaya, *Nature* **2002**, 419, 597.
- [81] M. Hanfland, K. Syassen, N. E. Christensen, D. L. Novikov, *Nature* **2000**, 408, 174.
- [82] J. B. Neaton, N. W. Ashcroft, *Nature* **1999**, 400, 141.
- [83] A. Rodriguez-Prieto, A. Bergara, V. M. Silkin, P. M. Echenique, *Phys. Rev. B* **2006**, 74, 172104.
- [84] N. E. Christensen, D. L. Novikov, *Phys. Rev. Lett.* **2001**, 86, 1861.
- [85] G. K. Straub, D. C. Wallace, *Phys. Rev. B* **1971**, 3, 1234.
- [86] R. J. Gooding, Y. Y. Ye, C. T. Chan, K. M. Ho, B. N. Harmon, *Phys. Rev. B* **1991**, 43, 13626.
- [87] T. Suzuki, H. M. Ledbetter, *Philos. Mag. A* **1983**, 48, 83.
- [88] W. Schwarz, O. Blaschko, I. Gorgas, *Phys. Rev. B* **1992**, 46, 14448.
- [89] R. Berliner, H. G. Smith, J. R. D. Copley, J. Trivisonno, *Phys. Rev. B* **1992**, 46, 14436.
- [90] A. Raju Natarajan, A. Van Der Ven, *Chem. Mater.* **2019**, 31, 8222.
- [91] O. Blaschko, V. Dmitriev, G. Krexner, P. Tolédano, *Phys. Rev. B* **1999**, 59, 9095.
- [92] A. W. Overhauser, *Adv. Phys.* **1978**, 27, 343.
- [93] G. H. Lander, E. S. Fisher, S. D. Bader, *Adv. Phys.* **1994**, 43, 1.
- [94] J. C. Marmeggi, G. H. Lander, S. Van Smaalen, T. Brückel, C. M. E. Zeyen, *Phys. Rev. B* **1990**, 42, 9365.
- [95] W. P. Crummett, H. G. Smith, R. M. Nicklow, N. Wakabayashi, *Phys. Rev. B* **1979**, 19, 6028.

- [96] H. G. Smith, N. Wakabayashi, W. P. Crummett, R. M. Nicklow, G. H. Lander, E. S. Fisher, *Phys. Rev. Lett.* **1980**, *44*, 1612.
- [97] L. Fast, O. Eriksson, B. Johansson, J. M. Wills, G. Straub, H. Roeder, L. Nordström, *Phys. Rev. Lett.* **1998**, *81*, 2978.
- [98] S. Raymond, J. Bouchet, G. H. Lander, M. Le Tacon, G. Garbarino, M. Hoesch, J.-P. Rueff, M. Krisch, J. C. Lashley, R. K. Schulze, R. C. Albers, *Phys. Rev. Lett.* **2011**, *107*, 136401.
- [99] E. Fawcett, *Rev. Mod. Phys.* **1988**, *60*, 209.
- [100] M. I. McMahon, R. J. Nelmes, *Chem. Soc. Rev.* **2006**, *35*, 943.
- [101] T. Aruga, *J. Phys.: Condens. Matter* **2002**, *14*, 8393.
- [102] T. Nakagawa, S. Mitsushima, H. Okuyama, M. Nishijima, T. Aruga, *Phys. Rev. B* **2002**, *66*, 085402.
- [103] J. M. Carpinelli, H. H. Weitering, E. W. Plummer, R. Stumpf, *Nature* **1996**, *381*, 398.
- [104] J. M. Carpinelli, H. H. Weitering, M. Bartkowiak, R. Stumpf, E. W. Plummer, *Phys. Rev. Lett.* **1997**, *79*, 2859.
- [105] H. W. Yeom, S. Takeda, E. Rotenberg, I. Matsuda, K. Horikoshi, J. Schaefer, C. M. Lee, S. D. Kevan, T. Ohta, T. Nagao, S. Hasegawa, *Phys. Rev. Lett.* **1999**, *82*, 4898.
- [106] J. Mohd Jani, M. Leary, A. Subic, M. A. Gibson, *Mater. Des.* **2014**, *56*, 1078.
- [107] W. J. Buehler, J. V. Gilfrich, R. C. Wiley, *J. Appl. Phys.* **1963**, *34*, 1475.
- [108] J. Mohd Jani, M. Leary, A. Subic, M. A. Gibson, *Mater. Des.* **2014**, *56*, 1078.
- [109] T. W. Duerig, *MRS Bull.* **2002**, *27*, 101.
- [110] T. Duerig, A. Pelton, D. Stöckel, *Mater. Sci. Eng., A* **1999**, *273-275*, 149.
- [111] G. F. Andreasen, T. B. Hilleman, *J. Am. Dent. Assoc.* **1971**, *82*, 1373.
- [112] D. J. Hartl, D. C. Lagoudas, *Proc. Inst. Mech. Eng., Part G* **2007**, *221*, 535.
- [113] J. Olbricht, A. Yawny, A. M. Condó, F. C. Lovey, G. Eggeler, *Mater. Sci. Eng., A* **2008**, *481-482*, 142.
- [114] Y. Chen, O. Molnárová, O. Tyc, L. Kadeřávek, L. Heller, P. Šittner, *Acta Mater.* **2019**, *180*, 243.
- [115] J. Frenzel, A. Wiczorek, I. Opahle, B. Maaß, R. Drautz, G. Eggeler, *Acta Mater.* **2015**, *90*, 213.
- [116] R. Delville, B. Malard, J. Pilch, P. Sittner, D. Schryvers, *Int. J. Plast.* **2011**, *27*, 282.
- [117] Ch. Grossmann, J. Frenzel, V. Sampath, T. Depka, A. Oppenkowski, Ch. Somsen, K. Neuking, W. Theisen, G. Eggeler, *Materialwiss. Werkstofftech.* **2008**, *39*, 499.
- [118] S. K. Patel, B. Swain, R. Roshan, N. K. Sahu, A. Behera, *Mater. Today: Proc.* **2020**, *33*, 5552.
- [119] Ch. Grossmann, J. Frenzel, V. Sampath, T. Depka, G. Eggeler, *Mater. Trans. A* **2009**, *40*, 2530.
- [120] K. C. Atli, B. E. Franco, I. Karaman, D. Gaydosch, R. D. Noebe, *Mater. Sci. Eng., A* **2013**, *574*, 9.
- [121] C. Chluba, W. Ge, R. Lima De Miranda, J. Strobel, L. Kienle, E. Quandt, M. Wuttig, *Science* **2015**, *348*, 1004.
- [122] H. Gu, L. Bumke, C. Chluba, E. Quandt, R. D. James, *Mater. Today* **2018**, *21*, 265.
- [123] R. E. McMahon, J. Ma, S. V. Verkhoturov, D. Munoz-Pinto, I. Karaman, F. Rubitschek, H. J. Maier, M. S. Hahn, *Acta Biomater.* **2012**, *8*, 2863.
- [124] K. Otsuka, X. Ren, *Prog. Mater. Sci.* **2005**, *50*, 511.
- [125] T. Waitz, *Acta Mater.* **2005**, *53*, 2273.
- [126] J. Khalil-Allafi, A. Dlouhy, G. Eggeler, *Acta Mater.* **2002**, *50*, 4255.
- [127] T. Inamura, H. Hosoda, S. Miyazaki, *Philos. Mag.* **2013**, *93*, 618.
- [128] H. Y. Kim, S. Miyazaki, *Ni-Free Ti-Based Shape Memory Alloys*, Butterworth-Heinemann, Oxford **2018**.
- [129] O. Benafan, D. J. Gaydosch, *Smart Mater. Struct.* **2019**, *28*, 085035.
- [130] S. Li, D. Cong, X. Sun, Y. Zhang, Z. Chen, Z. Nie, R. Li, F. Li, Y. Ren, Y. Wang, *Mater. Res. Lett.* **2019**, *7*, 482.
- [131] G. S. Firstov, T. A. Kosorukova, Y. N. Koval, V. V. Odnozum, *Mater. Today: Proc.* **2015**, *2*, S499.
- [132] J. Frenzel, G. Eggeler, E. Quandt, S. Seelecke, M. Kohl, *MRS Bull.* **2018**, *43*, 280.
- [133] S. Fähler, U. K. Röbler, O. Kastner, J. Eckert, G. Eggeler, H. Emmerich, P. Entel, S. Müller, E. Quandt, K. Albe, *Adv. Eng. Mater.* **2012**, *14*, 10.
- [134] S. Qian, Y. Geng, Y. Wang, J. Ling, Y. Hwang, R. Radermacher, I. Takeuchi, J. Cui, *Int. J. Refrig.* **2016**, *64*, 1.
- [135] M. Elahinia, N. Shayesteh Moghaddam, A. Amerinatanz, S. Saedi, G. P. Toker, H. Karaca, G. S. Bigelow, O. Benafan, *Scr. Mater.* **2018**, *145*, 90.
- [136] X. Wang, M. Speirs, S. Kustov, B. Vrancken, X. Li, J.-P. Kruth, J. Van Humbeeck, *Scr. Mater.* **2018**, *146*, 246.
- [137] S. A. Shabalovskaja, A. I. Lotkov, I. I. Sasovskaja, A. G. Narmonev, A. I. Zakharov, *Solid State Commun.* **1979**, *32*, 735.
- [138] S. A. Shabalovskaya, *Phys. Status Solidi B* **1985**, *132*, 327.
- [139] G.-L. Zhao, T. Leung, B. Harmon, M. Keil, M. Müllner, W. Weber, *Phys. Rev. B* **1989**, *40*, 7999.
- [140] N. Hatcher, O. Y. Kontsevoi, A. J. Freeman, *Phys. Rev. B* **2009**, *79*, 020202.
- [141] M. Zarinejad, Y. Liu, *Adv. Funct. Mater.* **2008**, *18*, 2789.
- [142] M. Zarinejad, Y. Liu, in *Shape Memory Alloys: Manufacture, Properties and Applications* (Ed: H. R. Chen), Nova Science Publishers, New York **2010**, p. 339–360.
- [143] T. Chakraborty, J. Rogal, R. Drautz, *Phys. Rev. B* **2016**, *94*, 224104.
- [144] A. Ferrari, D. G. Sangiovanni, J. Rogal, R. Drautz, *Phys. Rev. B* **2019**, *99*, 094107.
- [145] A. Ferrari, A. Paulsen, D. Langenkämper, D. Piorunek, C. Somsen, J. Frenzel, J. Rogal, G. Eggeler, R. Drautz, *Phys. Rev. Mater.* **2019**, *3*, 103605.
- [146] T. Krenke, E. Duman, M. Acet, E. F. Wassermann, X. Moya, L. Mañosa, A. Planes, *Nat. Mater.* **2005**, *4*, 450.
- [147] T. Graf, C. Felser, S. S. P. Parkin, *Prog. Solid State Chem.* **2011**, *39*, 1.
- [148] Y. Sutou, Y. Imano, N. Koeda, T. Omori, R. Kainuma, K. Ishida, K. Oikawa, *Appl. Phys. Lett.* **2004**, *85*, 4358.
- [149] R. Kainuma, W. Ito, R. Y. Umetsu, K. Oikawa, K. Ishida, *Appl. Phys. Lett.* **2008**, *93*, 091906.
- [150] I. Titov, M. Acet, M. Farle, D. González-Alonso, L. Mañosa, A. Planes, T. Krenke, *J. Appl. Phys.* **2012**, *112*, 073914.
- [151] T. Hickel, M. Uijtewaald, A. Al-Zubi, B. Dutta, B. Grabowski, J. Neugebauer, *Adv. Eng. Mater.* **2012**, *14*, 547.
- [152] O. I. Velikokhatnyi, I. I. Naumov, *Phys. Solid State* **1999**, *41*, 617.
- [153] A. Zheludev, S. M. Shapiro, P. Wochner, L. E. Tanner, *Phys. Rev. B* **1996**, *54*, 15045.
- [154] U. Stuhr, P. Vorderwisch, V. V. Kokorin, P.-A. Lindgård, *Phys. Rev. B* **1997**, *56*, 14360.
- [155] V. V. Kokorin, V. A. Chernenko, J. Pons, C. Segui, E. Cesari, *Solid State Commun.* **1997**, *101*, 7.
- [156] T. D. Haynes, R. J. Watts, J. Laverock, Z. Major, M. A. Alam, J. W. Taylor, J. A. Duffy, S. B. Dugdale, *New J. Phys.* **2012**, *14*, 035020.
- [157] Y. Lee, J. Y. Rhee, B. N. Harmon, *Phys. Rev. B* **2002**, *66*, 054424.
- [158] S. W. D'souza, A. Rai, J. Nayak, M. Maniraj, R. S. Dhaka, S. R. Barman, D. L. Schlagel, T. A. Lograsso, A. Chakrabarti, *Phys. Rev. B* **2012**, *85*, 085123.
- [159] B. T. Matthias, T. H. Geballe, S. Geller, E. Corenzwit, *Phys. Rev.* **1954**, *95*, 1435.
- [160] G. F. Hardy, J. K. Hulm, *Phys. Rev.* **1954**, *93*, 1004.
- [161] R. Mailfert, B. W. Batterman, J. J. Hanak, *Phys. Lett. A* **1967**, *24*, 315.
- [162] B. W. Batterman, C. S. Barrett, *Phys. Rev.* **1966**, *145*, 296.
- [163] L. R. Testardi, *Rev. Mod. Phys.* **1975**, *47*, 637.
- [164] M. Calandra, F. Mauri, *Phys. Rev. Lett.* **2011**, *106*, 196406.

- [165] M. Maschek, S. Rosenkranz, R. Hott, R. Heid, M. Merz, D. A. Zocco, A. H. Said, A. Alatas, G. Karapetrov, S. Zhu, J. Van Wezel, F. Weber, *Phys. Rev. B* **2016**, *94*, 214507.
- [166] A. Kogar, G. A. De La Pena, S. Lee, Y. Fang, S. X.-L. Sun, D. B. Lioi, G. Karapetrov, K. D. Finkelstein, J. P. C. Ruff, P. Abbamonte, S. Rosenkranz, *Phys. Rev. Lett.* **2017**, *118*, 027002.
- [167] D. Bhoi, S. Khim, W. Nam, B. S. Lee, C. Kim, B.-G. Jeon, B. H. Min, S. Park, K. H. Kim, *Sci. Rep.* **2016**, *6*, 24068.
- [168] M. Leroux, I. Errea, M. Le Tacon, S.-M. Souliou, G. Garbarino, L. Cario, A. Bosak, F. Mauri, M. Calandra, P. Rodière, *Phys. Rev. B* **2015**, *92*, 140303.
- [169] G. Monney, C. Monney, B. Hildebrand, P. Aebi, H. Beck, *Phys. Rev. Lett.* **2015**, *114*, 086402.
- [170] R. K. Bollinger, B. D. White, J. J. Neumeier, H. R. Z. Sandim, Y. Suzuki, C. A. M. Dos Santos, R. Avci, A. Migliori, J. B. Betts, *Phys. Rev. Lett.* **2011**, *107*, 075503.
- [171] M. O. Eatough, D. S. Ginley, B. Morosin, E. L. Venturini, *Appl. Phys. Lett.* **1987**, *51*, 367.
- [172] M. Fujita, H. Goka, K. Yamada, J. M. Tranquada, L. P. Regnault, *Phys. Rev. B* **2004**, *70*, 104517.
- [173] M. Hücker, M. V. Zimmermann, G. D. Gu, Z. J. Xu, J. S. Wen, G. Xu, H. J. Kang, A. Zheludev, J. M. Tranquada, *Phys. Rev. B* **2011**, *83*, 104506.
- [174] X. M. Chen, C. Mazzoli, Y. Cao, V. Thampy, A. M. Barbour, W. Hu, M. Lu, T. A. Assefa, H. Miao, G. Fabbris, G. D. Gu, J. M. Tranquada, M. P. M. Dean, S. B. Wilkins, I. K. Robinson, *Nat. Commun.* **2019**, *10*, 1435.
- [175] D. F. Agterberg, J. C. S. Davis, S. D. Edkins, E. Fradkin, D. J. Van Harlingen, S. A. Kivelson, P. A. Lee, L. Radzihovsky, J. M. Tranquada, Y. Wang, *Annu. Rev. Condens. Matter Phys.* **2020**, *11*, 231.
- [176] J. M. Tranquada, B. J. Sternlieb, J. D. Axe, Y. Nakamura, S. Uchida, *Nature* **1995**, *375*, 561.
- [177] R. Comin, A. Damascelli, *Annu. Rev. Condens. Matter Phys.* **2016**, *7*, 369.
- [178] A. Frano, S. C. Blanco, B. Keimer, J. R. Birgeneau, *J. Phys.: Condens. Matter* **2020**, *32*, 374005.
- [179] C. Proust, L. Taillefer, *Annu. Rev. Condens. Matter Phys.* **2019**, *10*, 409.
- [180] Y. Y. Peng, R. Fumagalli, Y. Ding, M. Minola, S. Caprara, D. Betto, M. Bluschke, G. M. De Luca, K. Kummer, E. Lefrançois, M. Salluzzo, H. Suzuki, M. Le Tacon, X. J. Zhou, N. B. Brookes, B. Keimer, L. Braicovich, M. Grilli, G. Ghiringhelli, *Nat. Mater.* **2018**, *17*, 697.
- [181] R. Arpaia, S. Caprara, R. Fumagalli, G. De Vecchi, Y. Y. Peng, E. Andersson, D. Betto, G. M. De Luca, N. B. Brookes, F. Lombardi, M. Salluzzo, L. Braicovich, C. Di Castro, M. Grilli, G. Ghiringhelli, *Science* **2019**, *365*, 906.
- [182] R. Comin, A. Frano, M. M. Yee, Y. Yoshida, H. Eisaki, E. Schierle, E. Weschke, R. Sutarto, F. He, A. Soumyanarayanan, Y. He, M. Le Tacon, I. S. Elfimov, J. E. Hoffman, G. A. Sawatzky, B. Keimer, A. Damascelli, *Science* **2014**, *343*, 390.
- [183] X. Zhu, Y. Cao, J. Zhang, E. W. Plummer, J. Guo, *Proc. Natl. Acad. Sci. USA* **2015**, *112*, 2367.
- [184] M. Le Tacon, A. Bosak, S. M. Souliou, G. Dellea, T. Loew, R. Heid, K.-P. Bohnen, G. Ghiringhelli, M. Krisch, B. Keimer, *Nat. Phys.* **2014**, *10*, 52.
- [185] J. Paglione, R. L. Greene, *Nat. Phys.* **2010**, *6*, 645.
- [186] Q. Si, R. Yu, E. Abrahams, *Nat. Rev. Mater.* **2016**, *1*, 16017.
- [187] D. C. Johnston, *Adv. Phys.* **2010**, *59*, 803.
- [188] A. E. Böhrner, A. Kreisel, *J. Phys.: Condens. Matter* **2017**, *30*, 023001.
- [189] J. H. Chu, H. H. Kuo, J. G. Analytis, I. R. Fisher, *Science* **2012**, *337*.
- [190] H.-H. Kuo, J.-H. Chu, J. C. Palmstrom, S. A. Kivelson, I. R. Fisher, *Science* **2016**, *352*, 958.
- [191] A. Dusza, A. Lucarelli, F. Pfüner, J.-H. Chu, I. R. Fisher, L. Degiorgi, *Europhys. Lett.* **2011**, *93*, 37002.
- [192] M. Fu, D. A. Torchetti, T. Imai, F. L. Ning, J.-Q. Yan, A. S. Sefat, *Phys. Rev. Lett.* **2012**, *109*, 247001.
- [193] S. Jiang, H. S. Jeevan, J. Dong, P. Gegenwart, *Phys. Rev. Lett.* **2013**, *110*, 067001.
- [194] M. Yi, D. Lu, J.-H. Chu, J. G. Analytis, A. P. Sorini, A. F. Kemper, B. Moritz, S.-K. Mo, R. G. Moore, M. Hashimoto, W.-S. Lee, Z. Hussain, T. P. Devereaux, I. R. Fisher, Z.-X. Shen, *Proc. Natl. Acad. Sci. USA* **2011**, *108*, 6878.
- [195] M. Yi, Y. Zhang, Z.-X. Shen, D. Lu, *npj Quantum Mater.* **2017**, *2*, 57.
- [196] T.-M. Chuang, M. P. Allan, J. Lee, Y. Xie, N. Ni, S. L. Bud'ko, G. S. Boebinger, P. C. Canfield, J. C. Davis, *Science* **2010**, *327*, 181.
- [197] R. M. Fernandes, A. V. Chubukov, J. Schmalian, *Nat. Phys.* **2014**, *10*, 97.
- [198] M. Yoshizawa, D. Kimura, T. Chiba, S. Simayi, Y. Nakanishi, K. Kihou, C.-H. Lee, A. Iyo, H. Eisaki, M. Nakajima, S.-I. Uchida, *J. Phys. Soc. Jpn.* **2012**, *81*, 024604.
- [199] A. E. Böhrner, P. Burger, F. Hardy, T. Wolf, P. Schweiss, R. Fromknecht, M. Reinecker, W. Schranz, C. Meingast, *Phys. Rev. Lett.* **2014**, *112*, 047001.
- [200] A. E. Böhrner, C. Meingast, *C. R. Phys.* **2016**, *17*, 90.
- [201] S. Yonezawa, *J. Phys.: Condens. Matter* **2019**, *4*, 2.
- [202] Y. Kohama, H. Ishikawa, A. Matsuo, K. Kindo, N. Shannon, Z. Hiroi, *Proc. Natl. Acad. Sci. USA* **2019**, *116*, 10686.
- [203] Y. Cao, D. Rodan-Legrain, J. M. Park, N. F. Q. Yuan, K. Watanabe, T. Taniguchi, R. M. Fernandes, L. Fu, P. Jarillo-Herrero, *Science* **2021**, *372*, 264.
- [204] S. Seo, X. Wang, S. M. Thomas, M. C. Rahn, D. Carmo, F. Ronning, E. D. Bauer, R. D. dos Reis, M. Janoschek, J. D. Thompson, R. M. Fernandes, P. F. S. Rosa, *Phys. Rev. X* **2020**, *10*, 011035.
- [205] F. Ronning, T. Helm, K. R. Shirer, M. D. Bachmann, L. Balicas, M. K. Chan, B. J. Ramshaw, R. D. McDonald, F. F. Balakirev, M. Jaime, E. D. Bauer, P. J. W. Moll, *Nature* **2017**, *548*, 313.
- [206] E. W. Rosenberg, J.-H. Chu, J. P. C. Ruff, A. T. Hristov, I. R. Fisher, *Proc. Natl. Acad. Sci. USA* **2019**, *116*, 7232.
- [207] S. Lederer, Y. Schattner, E. Berg, S. A. Kivelson, *Phys. Rev. Lett.* **2015**, *114*, 097001.
- [208] D. Labat, I. Paul, *Phys. Rev. B* **2017**, *96*, 195146.
- [209] W. Zhong, D. Vanderbilt, *Phys. Rev. B* **1996**, *53*, 5047.
- [210] D. Shin, S. Latini, C. Schäfer, S. A. Sato, U. De Giovannini, H. Hübener, A. Rubio, *Phys. Rev. B* **2021**, *104*, L060103.
- [211] P. M. Woodward, *Acta Cryst.* **1997**, *53*, 32.
- [212] R. A. Cowley, W. J. L. Buyers, G. Dolling, *Solid State Commun.* **1969**, *7*, 181.
- [213] H. Fujishita, S. Hoshino, *J. Phys. Soc. Jpn.* **1984**, *53*, 226.
- [214] Z. An, H. Yokota, N. Zhang, M. Paściak, J. Fábry, M. Kopecký, J. Kub, G. Zhang, A. M. Glazer, T. R. Welberry, W. Ren, Z.-G. Ye, *Phys. Rev. B* **2021**, *103*, 054113.
- [215] W. Cochran, *Adv. Phys.* **1960**, *9*, 387.
- [216] P. W. Anderson, *Fizika Dielektrikov* (Ed: G. I. Skanavi), Akad. Nauk SSSR Fizicheskii Inst. im P. N. Lebedeva, Moscow **1960**.
- [217] R. Comes, M. Lambert, A. Guinier, *Solid State Commun.* **1968**, *6*, 715.
- [218] A. S. Chaves, F. C. S. Barreto, R. A. Nogueira, B. Žekš, *Phys. Rev. B* **1976**, *13*, 207.
- [219] S. Tinte, M. G. Stachiotti, M. Sepiarsky, R. L. Migoni, C. O. Rodriguez, *Ferroelectrics* **2000**, *237*, 41.
- [220] B. Xu, O. Hellman, L. Bellaiche, *Phys. Rev. B* **2019**, *100*, 020102.
- [221] A. Bussmann-Holder, *J. Phys.: Condens. Matter* **2012**, *24*, 273202.
- [222] P. Garcia-Fernandez, J. A. Aramburu, M. T. Barriuso, M. Moreno, *J. Phys. Chem. Lett.* **2010**, *1*, 647.
- [223] R. E. Cohen, *Nature* **1992**, *358*, 136.
- [224] C. Enderlein, J. F. De Oliveira, D. A. Tompsett, E. B. Saitovitch, S. S. Saxena, G. G. Lonzarich, S. E. Rowley, *Nat. Commun.* **2020**, *11*, 4852.

- [225] W. Zhong, R. D. King-Smith, D. Vanderbilt, *Phys. Rev. Lett.* **1994**, *72*, 3618.
- [226] N. Marzari, A. A. Mostofi, J. R. Yates, I. Souza, D. Vanderbilt, *Rev. Mod. Phys.* **2012**, *84*, 1419.
- [227] P. B. Allen, *Phys. Rev. B* **1972**, *6*, 2577.
- [228] P. B. Allen, M. L. Cohen, *Phys. Rev. Lett.* **1972**, *29*, 1593.
- [229] J. D. Axe, G. Shirane, *Phys. Rev. Lett.* **1973**, *30*, 214.
- [230] S. M. Shapiro, G. Shirane, J. D. Axe, *Phys. Rev. B* **1975**, *12*, 4899.
- [231] D. E. Moncton, J. D. Axe, F. J. Disalvo, *Phys. Rev. B* **1977**, *16*, 801.
- [232] J. P. Pouget, B. Hennion, C. Escribe-Filippini, M. Sato, *Phys. Rev. B* **1991**, *43*, 8421.
- [233] G. Shirane, R. Nathans, V. J. Minkiewicz, *Phys. Rev.* **1967**, *157*, 396.
- [234] S. M. Shapiro, J. D. Axe, G. Shirane, T. Riste, *Phys. Rev. B* **1972**, *6*, 4332.
- [235] O. Delaire, J. Ma, K. Marty, A. F. May, M. A. Mcguire, M.-H. Du, D. J. Singh, A. Podlesnyak, G. Ehlers, M. D. Lumsden, B. C. Sales, *Nat. Mater.* **2011**, *10*, 614.
- [236] X. He, D. Bansal, B. Winn, S. Chi, L. Boatner, O. Delaire, *Phys. Rev. Lett.* **2020**, *124*, 145901.
- [237] R. F. Egerton, *Electron Energy-Loss Spectroscopy in the Electron Microscope*, Vol. XII, Springer, New York **2011**, p. 491.
- [238] C. Hébert, P. Schattschneider, *Ultramicroscopy* **2003**, *96*, 463.
- [239] P. Schattschneider, S. Rubino, C. Hébert, J. Ruzs, J. Kuneš, P. Novák, E. Carlino, M. Fabrizioli, G. Panaccione, G. Rossi, *Nature* **2006**, *441*, 486.
- [240] N. H. Dekkers, H. de Lang, *Optik* **1974**, *41*, 452.
- [241] K. J. O'shea, S. Mcvitie, J. N. Chapman, J. M. R. Weaver, *Appl. Phys. Lett.* **2008**, *93*, 202505.